Geochemistry and Geochronology of the Accreted Mafic Rocks From the Hengchun Peninsula, Southern Taiwan: Origin and Tectonic Implications

Article *in* Journal of Geophysical Research: Solid Earth · February 2019

DOI: 10.1029/2018JB016562

CITATION
1

READS
555

8 authors, including:

Tian Zhixian
Chinese Academy of Sciences
8 PUBLICATIONS **27** CITATIONS
SEE PROFILE

Yi Yan
Chinese Academy of Sciences
47 PUBLICATIONS **510** CITATIONS
SEE PROFILE

Chi-Yue Huang
National Cheng Kung University
107 PUBLICATIONS **3,046** CITATIONS
SEE PROFILE

Xinchang Zhang
Chinese Academy of Sciences
11 PUBLICATIONS **86** CITATIONS
SEE PROFILE

JGR Solid Earth

RESEARCH ARTICLE
10.1029/2018JB016562

Key Points:
- Ages of 22.8 +/- 0.3 and 24.2 +/- 1.1 Ma for N-MORBs from the SCS and 135.0 +/- 5.6 Ma for fragments of the Luzon forearc are obtained
- Accreted basalts in the Hengchun Peninsula record the subduction of the SCS accompanied by seamount and the consumption of Luzon forearc
- Alkaline OIBs from the South China Sea may record the contributions of recycled oceanic crust and the Hainan Plume

Supporting Information:
- Supporting Information S1
- Table S1
- Table S2
- Table S3
- Table S4
- Data Set S1

Correspondence to:
Y. Yan,
yanyi@gig.ac.cn

Citation:
Tian, Z.-X., Yan, Y., Huang, C.-Y., Zhang, X.-C., Liu, H.-Q., Yu, M.-M., et al. (2019). Geochemistry and geochronology of the accreted mafic rocks from the Hengchun Peninsula, southern Taiwan: Origin and tectonic implications. *Journal of Geophysical Research: Solid Earth*, *124*. https://doi.org/10.1029/2018JB016562

Received 16 AUG 2018
Accepted 10 FEB 2019
Accepted article online 15 FEB 2019

Geochemistry and Geochronology of the Accreted Mafic Rocks From the Hengchun Peninsula, Southern Taiwan: Origin and Tectonic Implications

Zhi-Xian Tian[1,2], Yi Yan[1,2], Chi-Yue Huang[1,3], Xin-Chang Zhang[1,2], Hai-Quan Liu[1,2], Meng-Ming Yu[1,4], Deng Yao[1,4], and Yildirim Dilek[5]

[1]Key Laboratory of Ocean and Marginal Sea Geology, Guangzhou Institute of Geochemistry, Chinese Academy of Sciences, Guangzhou, China, [2]Institutions of Earth Science, Chinese Academy of Sciences, Beijing, China, [3]School of Ocean and Earth Science, Tongji University, Shanghai, China, [4]College of Earth and Planetary Sciences, University of Chinese Academy of Sciences, Beijing, China, [5]Department of Geology and Environmental Earth Science, Miami University, Oxford, OH, USA

Abstract The accretionary prism of the Hengchun Peninsula at the southernmost tip of the active Taiwan orogen has newly emerged due to the transition from a subduction zone to an arc-continent collision zone. The mafic rocks within the Hengchun accretionary prism, whose provenance has long been controversial, are highly indicative of the mantle nature and tectonic evolution around the northern Manila Trench. Based on geochemical analyses, the accreted basalts are classified as normal and enriched mid-ocean ridge basalts (N-MORB and E-MORB) and alkaline ocean island basalts. The N-MORBs, which exhibit geochemical signatures indicative of virtually unmetasomatized depleted MORB mantle and yield zircon U-Pb ages of 22.8 ± 0.3 and 24.2 ± 1.1 Ma, were off-scraped from the subducted oceanic crust of the South China Sea (SCS). The alkaline ocean island basalts are considered fragments of subducted seamount due to their geochemical similarity with seamount basalts from the SCS. The Hf-Nd isotopic compositions of basalts from the north SCS may represent the contributions of recycled oceanic crust and the upwelling Hainan Plume. The E-MORBs, which exhibit similar geochemical compositions as rocks from the Huatung Basin and yield an $^{40}Ar/^{39}Ar$ age of 135.0 ± 5.6 Ma, were removed from the overriding plate due to the excessive shear stress between the converging plates and were laterally transported by strike-slip movement; alternatively, they were off-scraped from the subducted Luzon forearc slices. The temporary uplift and collapse of the accretionary prism caused by seamount subduction may have been responsible for the genesis of the lenticular Shihmen Conglomerate.

1. Introduction

The vast majority of a subducting plate, including oceanic lithosphere, igneous seamounts, overlying polygenic sediments and fluids, will enter the deep mantle, while a minor part of the subducting plate will be scraped off and transferred to the forearc domain of the overriding plate. The off-scraped material accumulates in an accretionary prism (accretionary wedge) located directly at the convergent boundary through frontal accretion and underplating (Meschede, 2014). An accretionary prism represents the key link between plate tectonics and orogenesis, and its structures and components can be used to clarify the geodynamic histories of convergent plates and the tectonic-geomorphic evolution of adjacent areas (C. Y. Huang et al., 2012; Lan et al., 2015). More importantly, the accreted mafic rocks within accretionary prisms are the only acquirable samples of subducted oceanic crust and igneous seamounts; thus, they are valuable for revealing the mantle nature of convergent plates and constraining regional magmatic histories (Ker et al., 2015; Safonova et al., 2016).

Taiwan Island, which is located along the convergent boundary between the Huatung-Philippine Sea Plate and the Eurasian Plate (Figure 1), was generated by the subduction of the South China Sea (SCS) and the subsequent arc-continent collision between the South China continental margin and the north Luzon arc (C. Y. Huang et al., 2012). A series of NE trending rift basins opened due to the extension occurred along the eastern Eurasian continental margin in the early Cenozoic (P. Li & Rao, 1994). Among these, the SCS, which opened during the early Oligocene-middle Miocene, is the largest marginal sea in the western Pacific (C. Y. Huang et al., 2001). Immediately after the cessation of seafloor spreading, the oceanic crust of the SCS subducted eastward beneath the Huatung-Philippine Sea Plate at the Manila Trench, resulting

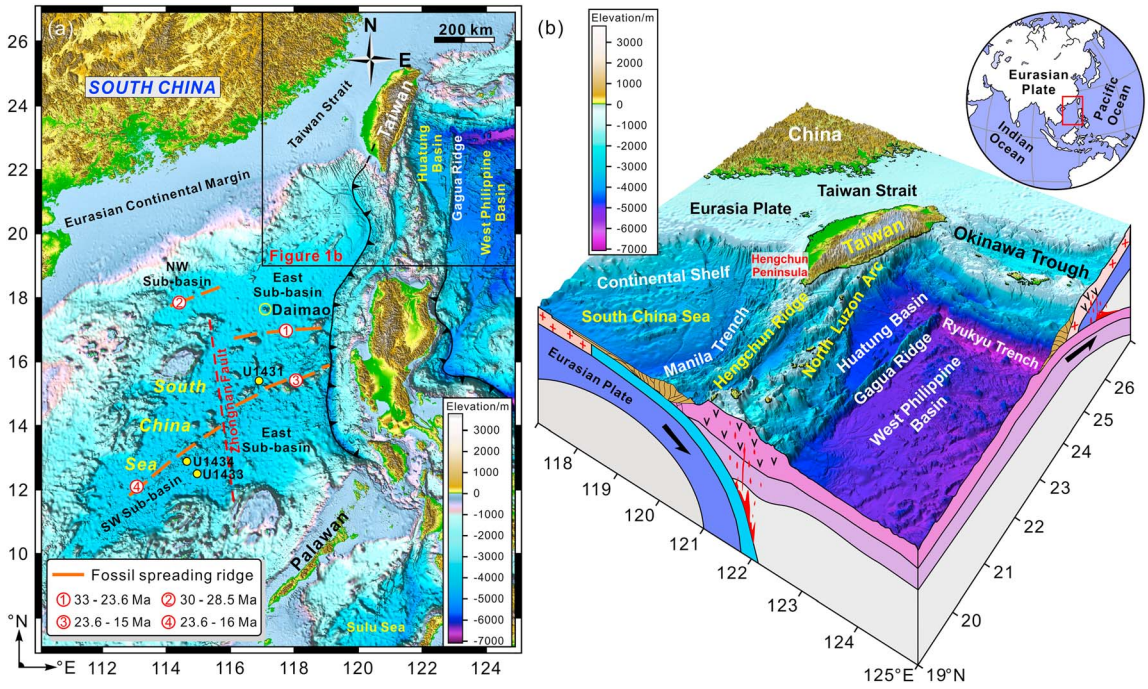

Figure 1. Regional tectonic and topographic sketch map of the Taiwan Orogen and the adjacent areas (a; after Yu et al., 2018). Block diagram showing the arc–continent collision and tectonic setting of Taiwan, between the Eurasian continent and the Huatung-Philippine Sea Plate (b).

in the formation of an accretionary wedge and the north Luzon arc (Lai et al., 2017; Song & Lo, 2002). Meanwhile, the Huatung-Philippine Sea Plate began subducting beneath the Eurasian Plate toward the NW at a rate of 82 km/m.y. along the Ryukyu Trench (Lewis et al., 2015). Because the boundary between the oceanic and continental crust at the northern margin of the SCS trends differently from both the Manila Trench and the north Luzon arc (C. Y. Huang et al., 2000), the transition from intraoceanic subduction to continental subduction has migrated southward, and the orogenesis induced by oblique arc-continent collision has propagated to the SSW at ~60 km/m.y. (C. Y. Huang et al., 1997; Lewis et al., 2015).

The Hengchun Peninsula in southern Taiwan marks the latest exposed part of the accretionary prism in the Northern Manila subduction zone. At the intraoceanic subduction stage (Figure 2), the Hengchun accretionary prism (Hengchun Ridge) widened and thickened due to sediment deformation and off-scraping. Further, as it proceeded into the initial arc-continent collision stage, it was uplifted and became subaerially exposed since ~4 Ma (C. Y. Huang et al., 2006). The newly emerged Hengchun accretionary contains abundant mafic rocks, which vary in their lithology and scale and exhibit different degrees of roundness, alteration, and metamorphism. The geochemistry and chronology of these accreted mafic rocks are critical indicators of the provenance and geodynamic evolution of the accretionary prism and can help constrain the regional magmatic history and nature of the mantle around the convergent boundary. However, direct studies of these accreted basalts are quite limited (H. Y. Chen et al., 2018; Page & Lan, 1983; Pelletier & Stephan, 1986), and interpretations of their provenance based on the paleobiology of their accompanying sediments, structural analysis, and regional geophysics remain speculative and controversial (Byrne, 1998; C. P. Chang et al., 2003; C. Y. Huang, 1984; Malavieille et al., 2016; X. C. Zhang et al., 2016). In early studies, accreted basaltic rocks were often regarded as fragments of the oceanic crust of the SCS (C. Y. Huang et al., 1985; Muller et al., 1984; Page & Lan, 1983; Pelletier & Stephan, 1986). The igneous pebbles within the turbidite sequences have even been interpreted to be derived from the South China continent together with fine-grained sediments. According to the latest research conducted by H. Y. Chen et al. (2018), both the subducting and overriding plates are involved in the provenances of the accreted basalts. However, the origin of the alkaline ocean island basalts (OIBs) remains ambiguous, and the possibility of components being derived from the West Philippine Basin east of the Gagua Ridge (Figure 1b), which contradict the tectonic setting, appears to be impossible. Consequently, the formation mechanisms of the ophiolite-bearing stratigraphic

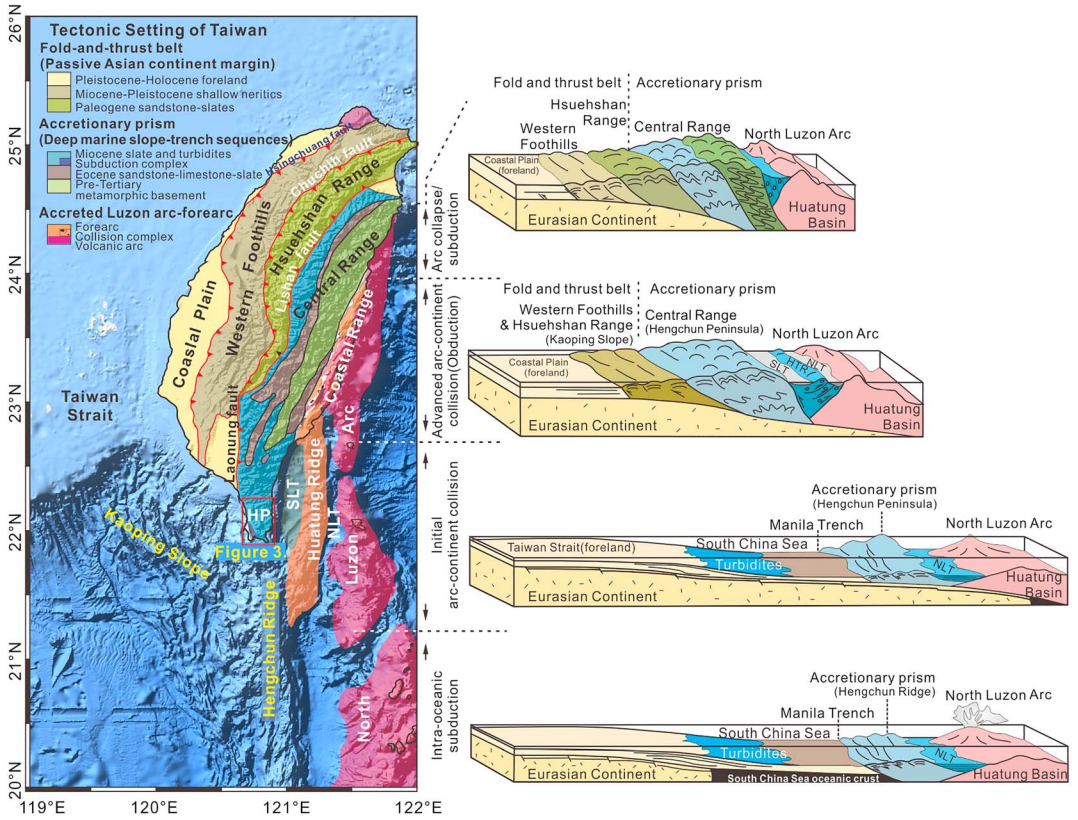

Figure 2. Simplified stratigraphic map and tectonic evolution of Taiwan. Four tectonic processes are now operating onland Taiwan and its offshore regions. From south to north they are: Intraoceanic subduction, initial arc-continent collision, advanced arc-continent collision, and arc collapse/subduction (C. Y. Huang et al., 2012). HP = Hengchun Peninsula; SLT = Southern Longitudinal Trough; HTR = Huatung Ridge; NLT = North Luzon Trough.

units, including the Kenting Mélange, the Shihmen Conglomerate, the Cingwashih slump deposits and the Lilungshan Sandstone, are still unclear.

In this work, we conducted an integrated study of the geochemistry, geochronology, and Hf-Nd isotopic compositions of the basaltic rocks collected from the Hengchun Peninsula to address the following specific questions: Do basaltic fragments of the overriding plate exist in the Hengchun accretionary prism? What implications can the accreted basalts provide about the nature of the mantle and the tectonic evolution in the northern Manila subduction zone? Did the igneous pebbles within the turbidite sequences come from the Chinese continent, or can they be attributed to the sediment recycling of the accretionary prism?

2. Geologic Setting

The active Taiwan orogen comprises five geomorphic units that can be assigned to three NS trending structural belts from west to east (Figure 2); these include the fold and thrust belt on the passive Eurasian continental margin (Coastal Plain, Western Foothills, and Hsuehshan Range); the accretionary wedge (Central Range-Hengchun Peninsula); and the accreted Luzon arc-forearc (Coastal Range; C. Y. Huang et al., 2006). The Hengchun Ridge-Hengchun Peninsula-Central Range region comprises the accretionary prism of the Manila subduction system (Figure 2). The arc and forearc domains are directly juxtaposed to the Central Range in the form of the Coastal Range along the Longitudinal Valley fault system (C. P. Chang et al., 2003; C. Y. Huang et al., 1997), which extends offshore to the collision suture basin (Southern Longitudinal Trough; SLT in Figure 2), separating the forearc basin (Huatung Ridge) to the east and the accretionary wedge (Hengchun Peninsula-Hengchun Ridge) to the west (Byrne, 1998; C. Y. Huang et al., 2000; X. C. Zhang et al., 2016). The NW-SE oriented submarine Kaoping Slope, to the west of the Hengchun accretionary wedge, represents the developing collision prism associated with the incipient arc-continent collision (C. Y. Huang et al., 2006). To the west of the Kaoping Slope, the northernmost

Manila Trench is poorly defined and turns to the leading edge of the deformation of the collision prism (C. Y. Huang et al., 2000). The Huatung-Philippine Sea Plate, which is located to the east of the Hengchun Peninsula, is further divided into the Huatung Basin (early Cretaceous, 131–119 Ma) and the West Philippine Basin (early Eocene to early Oligocene, 55–33/30 Ma; Deschamps & Lallemand, 2002; Deschamps et al., 2000) by the Gagua Ridge (Figure 1b), which is a strike-slip feature that has accommodated the opening of the West Philippine Basin and been uplifted due to the compressive episode of a failed subduction event occurred along the western margin of the West Philippine Basin during the late Eocene-early Oligocene (Deschamps et al., 2000; Deschamps & Lallemand, 2002; Eakin et al., 2015).

As an active arc-continent collision orogen, Taiwan Island exhibits different tectonic evolution stages from north to south (Figure 2; C. Y. Huang et al., 1997). The Hengchun Peninsula, which is located at the southernmost tip of Taiwan Island and extends southward to the submarine Hengchun Ridge, is the southern extension of the Central Range (C. Y. Huang et al., 1997; C. Y. Huang et al., 2000). As a newly emerged accretionary prism, this region exhibits the youngest and best preserved accretionary sequences in Taiwan (C. P. Chang et al., 2003). The Hengchun Peninsula is an ideal natural laboratory for research of the internal structures of accretionary prisms and the transition from subduction—accretion to collision—orogenesis systems; it is thus ideal for clarifying the tectonic evolution of Taiwan and the subduction of the SCS (C. Y. Huang et al., 2006; Shan et al., 2013). Three tectonostratigraphic units, which are divided by the Hengchun Fault and the Kenting Fault, are recognized in the Hengchun Peninsula (Figure 3a):

The Hengchun accretionary prism mainly consists of thick middle to late Miocene turbiditic sequences (N14–N17; L. S. Chang, 1964), which have been folded and overturned westward and thrust upon the Kenting Mélange along the Kenting Fault. The sediments that accumulated in the accretionary wedge were off-scraped from the subducted SCS oceanic lithosphere and originally sourced from southeast China (Kirstein et al., 2010; X. C. Zhang et al., 2014). The turbidite sequences can be considered a single stratigraphic unit, namely, the Mutan Formation (C. P. Chang et al., 2003). This major formation is primarily composed of alternating siltstones and sandstones, with numerous sandstone and conglomerate lenses at various scales (Figure 3a). The major lentiform bodies intercalated in the Mutan Formation include the following: (a) The Lilungshan Sandstone (Mtl), which is interfingered with the underlying Mutan Formation. It exhibit a coarsening and thickening upward sequence from thin sandy turbidites to thick sandstones and finally to conglomerates (X. C. Zhang et al., 2014). Therefore, the Lilungshan Sandstone is considered the upper member of a submarine fan deposits, while part of the underlying Mutan Formation represents the lower part of the same submarine deposits (S. B. Lin & Wang, 2001). (b) The Shihmen Conglomerate (Mtk), with the Ssuchungchi Gorge (SG) as a representative outcrop and the slump deposits in Cingwashih area as fragments of it, is characterized by the dominance of magmatic components and is predominantly composed of thick-bedded channel-fill deposits (i.e., conglomerate) with subordinate sandstones (S. B. Lin & Wang, 2001; X. C. Zhang et al., 2014). The well-sorted pebbles within the Shihmen Conglomerate are generally clast supported, with the clast components composed of sand, as well as rock fragments and feldspar, which are likely produced by mutual abrasion between the igneous blocks. The subordinate sandstones are generally poorly to moderately sorted and contain a large proportion of silt, granules and fine gravels, with the cementation types predominantly include calcium cementation, followed by clay mineral cementation. (c) The Loshui Sandstone (Mtg) consists mainly of thick fine- to medium-grained sandstone beds and sandy turbidite layers, with minor amounts of igneous detritus (Kirstein et al., 2010; X. C. Zhang et al., 2014). The compositions of the conglomerate and igneous detritus within these lentiform bodies are mainly basalt, gabbro, diabase, and meta-basaltic rocks. Additionally, well-preserved fossils and fossil fragments, including oyster, conch, and leaves, are common in these lenticular bodies. Based on the combination of their petrography and suspected paleocurrent directions, which are from NW to SE in the Lilungshan Sandstone and from SE to NW in the Loshui Sandstone, distinct origins for these lenticular bodies have been proposed (Kirstein et al., 2010; Sung & Wang, 1986; X. C. Zhang et al., 2014).

To the west of the Hengchuan Fault, the western Hengchun Platform, which dips slightly to the east, is composed of the Plio-Pleistocene foreland sequences deposited in a progressively shallowing marine sedimentary environment (Figure 3; C. P. Chang et al., 2003). The Maanshan Formation (3.7–1 Ma), which unconformably overlies the Miocene turbidites, is generally considered to represent the slope basin sequences deposited after the commencement of arc-continent collision (C. Y. Huang et al., 2012). The microfossil assemblages recovered from the base of the Maanshan Formation (N19 or NN15, 3.7–3.5 Ma)

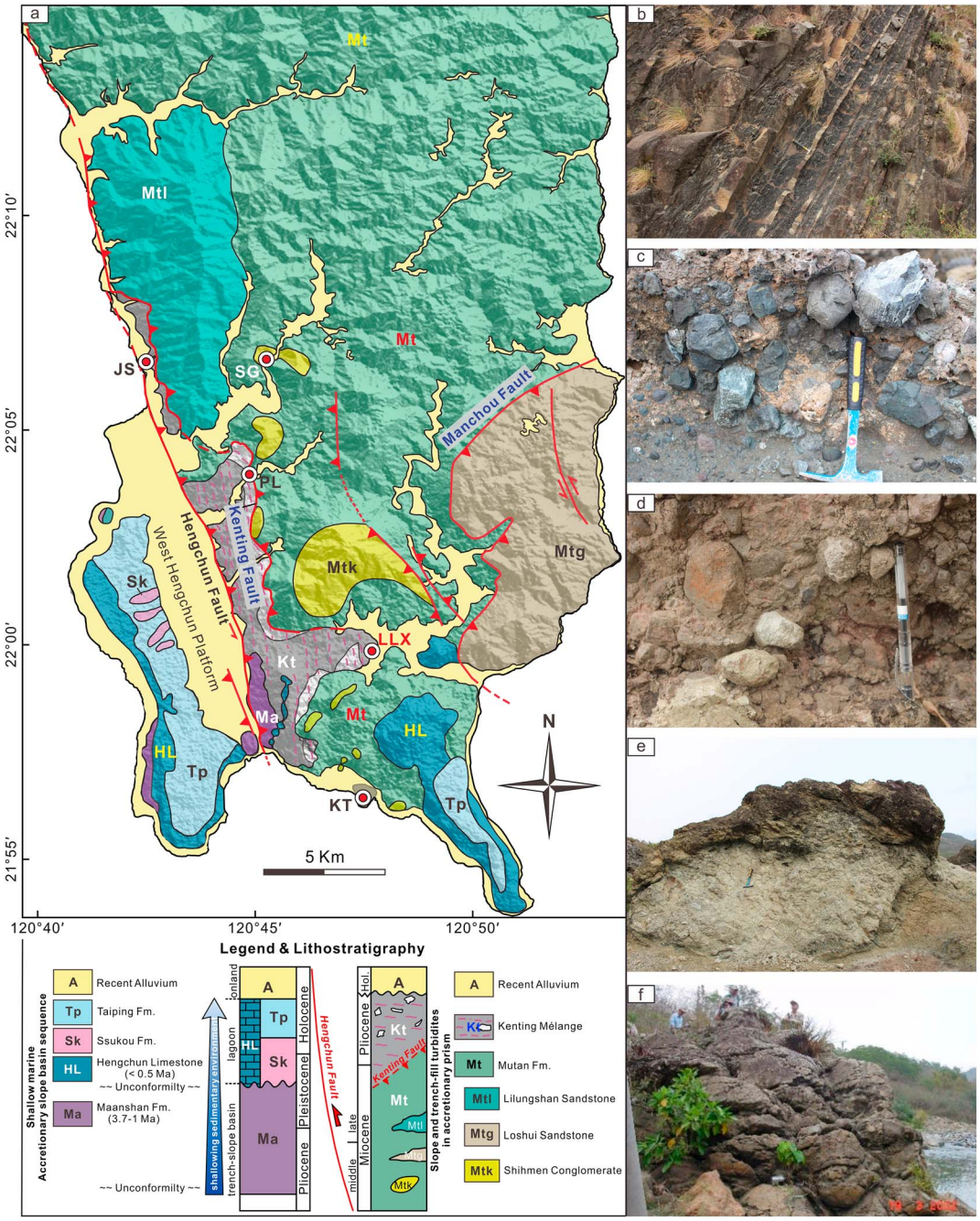

Figure 3. Simplified geological map of the Hengchun Peninsula (a) modified after C. P. Chang et al. (2003) and Giletycz et al. (2015) and representative field photographs from the Hengchun area: outcrop of the flysch sequences in the turbiditic Mutan Formation (b); Igneous pebbles rounded and metamorphosed to different degrees (c); Angular basalt block in the Jianshan area (d); Massive gabbro block in the Kenting area (e); and Pillow basalt in the Ssuchungchi Gorge (f). The stratigraphic column is modified after Giletycz et al. (2017). Abbreviations: KT = Cingwashih Park in the Kenting area; SG = Ssuchungchi Gorge; PL = Paoli area; LLX = Liangluanxi area; JS = Jianshan area.

suggest that the arc-continent collision in the Hengchun Peninsula could have started at ~4 Ma (C. Y. Huang et al., 2006). The siliciclastic Maanshan Formation is unconformably overlain by the eastward dipping reef-lagoonal complex and fluvial deposits (latest Pleistocene, <0.5 Ma), implying that the slope basin was recently uplifted and deformed (C. Y. Huang et al., 2006).

The Kenting Mélange, which crops out in a narrow area of badland between the Hengchun Fault and the Kenting Fault (Figure 3a), is a chaotic unit characterized by polygenic clasts ranging in size from a few

centimeters to hundreds of meters embedded in argillaceous matrix (C. P. Chang et al., 2009). From east to west, there is a structural gradation in the Kenting Mélange from folded stratified turbidite sequences against the Mutan Formation to similar sediments with disrupted strata (broken formation) and, finally, to fully developed mélange consisting of igneous blocks and argillaceous sediments (Page & Lan, 1983; X. C. Zhang et al., 2016). The argillaceous matrix is pervasively sheared and exhibits no discernible stratification, with scaly foliation as its most common mesoscopic structure. The curved scaly foliation surfaces are generally smoothed and bear slickenside lineations and minerals with preferred orientations, which reveal the sense and direction of shearing (C. P. Chang et al., 2003). The rock blocks and fragments in the Kenting Mélange can be classified into two genetic types: sedimentary and igneous. The sedimentary fragments consist of siltstones, sandstones, conglomerates, and limestones (rare), and most of them are autochthonous (C. P. Chang et al., 2009). The igneous blocks are mainly composed of basalts, gabbros, amphibolites, diabases, and volcanic breccias (C. Y. Huang et al., 1985; S. B. Lin & Wang, 2001; X. C. Zhang et al., 2016).

3. Sample Locations and Petrology

The accreted mafic rocks in the Hengchun Peninsula include differently rounded pebbles and massive blocks. The igneous pebbles are composed of (in decreasing abundance) basalt, gabbro, diabase, and amphibolite, and they can be further divided into the following: (a) well-sorted, subangular to rounded pebbles in the Shihmen Conglomerate and the slump deposits in Cingwashih area (Figure 3c); and (b) angular to subangular igneous pebbles in the Kenting Mélange (Figure 3d), which are generally poorly sorted. The massive igneous blocks associated with the pebbles show significant variations in size, for example, one of the gabbro blocks in the slump deposits at Cingwashih is approximately 3 m wide (Figure 3e), and the pillow basalts exposed in the Ssuchungchi Gorge (Figure 3f) and the Liangluanxi area can reach up to tens of meters in length. Additionally, chloritization and epidotization resulted from seafloor hydrothermal alteration and/or accretion-related metamorphism are common in the accreted basalts.

Forty-four relatively fresh samples were collected from the Kenting Mélange and the Shihmen Conglomerate: Seventeen samples, including gabbro, diabase, basalt, and amphibolite, were collected from the slump deposits in Cingwashih Park in the Kenting area (KT). Six samples of basalt, diabase porphyrite, and coarse-grained gabbro were obtained from the Jianshan area (JS), which is a representative outcrop of the Kenting Mélange. Eight samples including pillow basalt, gabbro, diabase, and amphibolite were collected from the Shihmen Conglomerate exposed in the Ssuchungchi Gorge (SG). Six pieces of basalt and diabase samples were collected from the Kenting Mélange along the Paoli river (PL). Seven samples of pillow basalt were collected from the Liangluanxi area (LLX).

Petrographically, the unmetamorphosed rocks can be categorized as phyric to moderately aphyric, while the amphibolites are characterized by crystalloblastic textures. Most gabbro samples show typical gabbroic textures (Figure 4a): Similar sized hypautomorphic granular pyroxene and feldspar crystals are irregularly arranged and cross each other. It is common to see fine-grained (0.3–0.5 mm) plagioclase produced by earlier crystallization trapped in late-crystallized pyroxene, thus forming poikilitic textures (Figures 4a and 4b). Some gabbro samples show gabbroic-ophitic textures in which plagioclase crystals are larger and more idiomorphic than pyroxene crystals (Figure 4b). Diabases generally exhibit typical ophitic textures, with idiomorphic plagioclase crystals forming triangular or square grids filled by anhedral pyroxene crystals (Figure 4c). As the most common metamorphic rock type, amphibolite is considered to represent metamorphosed gabbro or diabase (Page & Lan, 1983). Streaky structured amphibolites have crystalloblastic textures with elongated minerals exhibiting a preferred orientation (Figure 4d). Diabase porphyrite from the Jianshan area show porphyritic-like textures, with phenocrysts of plagioclase reaching up to 5 mm in size in the ophitic groundmass (Figure 4e). Pillow basalts with vesicles and amygdales from the Ssuchungchi Gorge and the Liangluanxi area have cryptocrystalline or intersertal textures, with amphibole crystals having undergone talcization and plagioclase crystals up to 0.6 mm long in the aphanitic groundmass (Figure 4f).

4. Analytical Methods

Samples were initially cleaned and crushed into small grains of approximately 5 mm in diameter. Fresh grains with no visible weathered surfaces or secondary minerals were immersed in 3% HCl for 20 min and

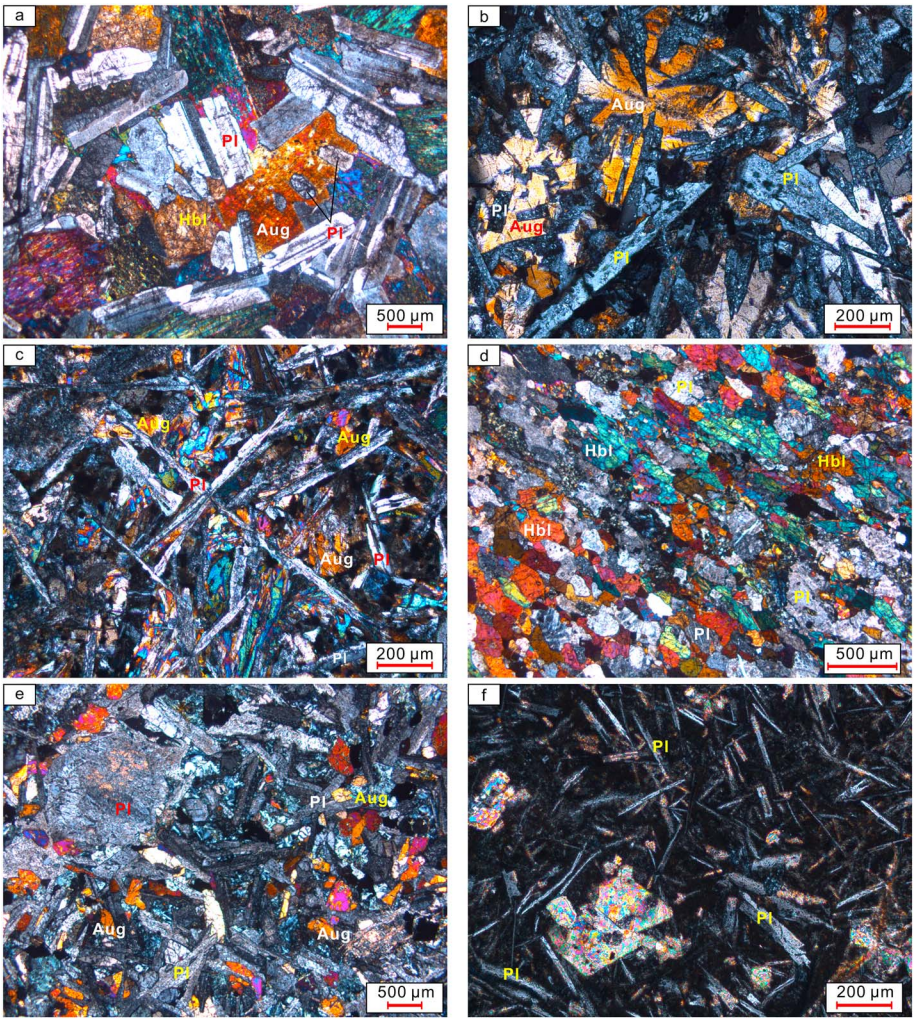

Figure 4. Photomicrographs illustrating the rock textures and mineralogy of the accreted mafic rocks from the Hengchun Peninsula: Gabbro sample KT03, with gabbroic texture and poikilitic texture (a); Gabbro with gabbroic-ophitic texture (b, sample KT11); Diabase with ophitic texture (c, sample KT06); Oriented minerals in amphibolite with crystalloblastic texture (d, sample KT10); Plagioclase phenocryst and ophitic textured matrix in diabase porphyrite sample (e, sample JS01); and Pillow lava with intersertal texture (f, sample LLX3). Pl = plagioclase; Aug = augite; Hbl = hornblende.

washed with deionized water three times in an ultrasonic cleaner. Leached grains were dried in an oven and pulverized into powders with a particle size of 200 mesh with a tungsten carbide mortar.

Major element analyses were conducted using a Rigaku ZSX100e X-ray fluorescence on fused glass beads at the State Key Laboratory of Isotope Geochemistry, Guangzhou Institute of Geochemistry, Chinese Academy of Sciences (GIGCAS). Detailed analytical procedures were described by Yuan et al. (2010). Calibration curves produced by the bivariate regression of data from 36 reference materials encompassing a wide range of silicate compositions were used for quantification (X. H. Li, 2003), and the analytical uncertainties ranged from 1% to 5%.

The concentrations of trace elements, including those of rare earth elements (REEs), were obtained using a Perkin-Elmer ELAN-DRC-e inductively coupled plasma mass spectrometer (ICP-MS) at the State Key Laboratory of Ore Deposit Geochemistry, Institute of Geochemistry, Chinese Academy of Sciences, following the detailed procedures described by Liang et al. (2000) and Qi and Zhou (2008).

Zircon grains were separated from two amphibolite samples using magnetic separation and heavy liquid techniques, followed by handpicking under a binocular microscope. The grains were mounted in transparent epoxy resin and then polished to expose their interiors. To identify the internal structures of the zircons

and choose target sites for U-Pb analyses, all grains were studied using cathodoluminescence (CL) imaging at the GIGCAS, using a CAMECA electron microprobe. SIMS (secondary ion mass spectrometry) zircon U-Pb dating was conducted using a CAMECA IMS-1280 ion microprobe (CASIMS) at the Institute of Geology and Geophysics, Chinese Academy of Sciences, following the procedures described by X. H. Li et al. (2009). The contents of U, Th, and Pb and their isotopic ratios were corrected relative to those of the standard zircon 91500 (1065.4 ± 0.6 Ma; Wiedenbeck et al., 1995). Concordia diagrams and weighted mean plots were derived using the Isoplot 4.15 (Ludwig, 2008).

$^{40}Ar/^{39}Ar$ dating was conducted at the $^{40}Ar/^{49}Ar$ Geochronology Laboratory, Institute of Geology and Geophysics, Chinese Academy of Sciences. Approximately 500 mg of fresh plagioclase crystals was packaged in aluminum foil and loaded into a quartz tube (25-mm-long × 5-mm inner diameter) with the Ga1550 biotite crystals (98.79 ± 0.96 Ma; Renne et al., 1998) as the neutron flux monitor. The tube was sealed with 0.5-mm-thick cadmium film and irradiated in the 49-2 reactor. Incremental heating for argon extraction was performed using an external temperature-controlled oven. The extracted gas was purified using two SAES (Società Apparecchi Elettrici e Scientifici) NP10 Zr-Al getters and a liquid nitrogen condensation trap; it was then analyzed on a MM5400 mass spectrometer. The argon isotopic data were calculated and plotted with the ArArCalc software (Koppers, 2002). The detailed procedures followed those of Qiu and Jiang (2007) and L. Yang et al. (2014).

The measurements of Hf-Nd isotopic ratios were performed at the GIGCAS using a Neptune Plus multicollector ICP-MS. The detailed analytical procedures were similar to those described by X. H. Li et al. (2007) and Ma et al. (2013). Hf-Nd isotopic fractionations were corrected using values of $^{179}Hf/^{177}Hf = 0.7325$ and $^{146}Nd/^{144}Nd = 0.7219$, respectively. Reference standards were analyzed in alternation with samples and yielded a value of $^{143}Nd/^{144}Nd = 0.512111 \pm 0.000003$ (2σ, $n = 7$) for Shin Etsu JNdi-1 and a value of $^{176}Hf/^{177}Hf = 0.282194 \pm 0.000007$ (2σ, $n = 7$) for JMC14374. These values are in accordance with their documented values (Tanaka et al., 2000; Wu et al., 2006) within a reasonable error range, thus justifying the accuracy of these measurements. The Geological Survey of Japan rock reference JB-3 was treated and analyzed along with the samples and yielded values of $^{143}Nd/^{144}Nd = 0.513051 \pm 5$ (2σ) and $^{176}Hf/^{177}Hf = 0.283235 \pm 4$ (2σ), which are consistent with their reported values (X. H. Li et al., 2005; Orihashi et al., 1998), indicating that these isotopes were extracted correctly and were free of contamination.

5. Results

5.1. Effects of Alteration and Metamorphism on Element Mobility

The major and trace element contents obtained for the accreted basalt samples are presented in Table S1 in the supporting information. To enable comparisons between samples and to exhibit the data graphically, the major element contents are normalized to 100 wt.% on an anhydrous basis. The accreted mafic rocks show both alkaline and subalkaline affinities and plot in the fields of basalt, basaltic andesite, andesite, trachybasalt, basaltic trachyandesite, and trachyandesite on the total alkalis versus silica diagram (Figure 5a; Le Maitre, 2002). The wide variations in major elements suggest that the accreted mafic rocks represent a magmatic series generated in different tectonic settings. However, the analyzed samples from the convergent plate boundary have undergone seafloor hydrothermal alteration and accretion-related regional metamorphism and then have been diagenetically altered to some extent (Saito et al., 2015). The contents of SiO_2, K_2O, Na_2O, FeO, and MgO in these rocks would probably have been distorted by these processes. The loss on ignition values of all samples vary widely from 0.54 to 9.96 wt.%. Thus, the major element concentrations of the accreted basalts are unlikely to be pristine and are thus not suitable indicators with which to constrain their provenances (Khogenkumar et al., 2016). For instance, Page and Lan (1983) argued that the alkaline affinity shown by some mafic rocks is not real and should instead be ascribed to their alkali enrichment and silica depletion caused by later alteration.

Even the large ion lithophile element (LILE, e.g., Rb, Ba, K, Sr, Pb, and Cs) contents of the accreted basalts exhibit no meaningful trends (Table S1), which is indicative of their diverse mobilization during hydrothermal alteration and metamorphism (Khogenkumar et al., 2016; Safonova et al., 2016; Said & Kerrich, 2009; Saito et al., 2015; Shervais, 1982). In contrast, based on many studies of Archean rocks and seafloor basalts, it is well accepted that Al_2O_3, TiO_2, P_2O_5, high field-strength elements (HFSE, e.g., Th, Nb, Ta, Zr, Hf, Y, and REEs), and some transition elements (e.g., Ni, Cr, Co, Sc, and V) are relatively immobile during

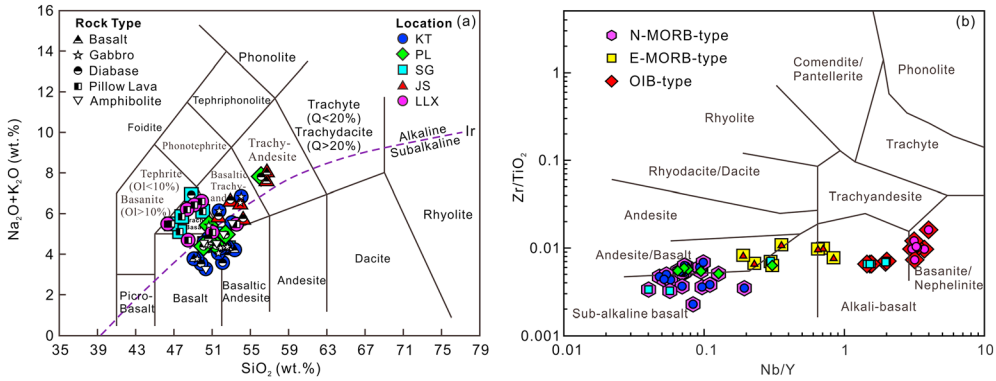

Figure 5. Tectonic discrimination diagrams for the accreted mafic rocks collected from the Hengchun accretionary prism: (a) total alkalis versus silica diagram (Le Maitre, 2002) and (b) Zr/TiO_2 versus Nb/Y diagram (Winchester & Floyd, 1977). N-MORB = normal mid-ocean ridge basalt; E-MORB = enriched mid-ocean ridge basalt; OIB = ocean island basalt.

metamorphism and alteration (Beccaluva et al., 1979; Bi et al., 2017; Pearce & Norry, 1979; Said & Kerrich, 2009). The mobility of light REEs may also indicate that they are more sensitive to secondary processes than heavy REEs but that only occurs with high fluid/rock ratios or during carbonatization (Humphris, 1984), which is not observed in our study. Accordingly, we will constrain the provenance of the accreted mafic rocks within the Hengchun accretionary prism using the contents of elements that are insensitive to alteration and metamorphism.

5.2. Major and Trace Element Geochemistry

These rocks plot in the fields of andesite/basalt and basanite/nephelinite on the Zr/TiO_2 versus Nb/Y classification diagram (Figure 5b; Winchester & Floyd, 1977). Although several samples show a conversion from alkaline to subalkaline affinities or the reverse, both affinities do exist among the mafic rocks from the Hengchun Peninsula. Therefore, despite the slight redistribution of mobile elements induced by alteration and metamorphism, the identification of protoliths based on the concentrations of K_2O, Na_2O and SiO_2 in most samples is reliable. Based on their geochemical variations (Table S1), specifically, the differences in their contents of incompatible elements, the analyzed samples can generally be classified into three major groups, namely, normal mid-ocean ridge basalt (N-MORB)-type, enriched mid-ocean ridge basalt (E-MORB)-type, and OIB-type rocks.

5.2.1. N-MORB Type

The N-MORB-type rocks comprise samples collected from the Kenting, Ssuchungchi, and Paoli areas, including diabases, gabbros, basalts, and amphibolites. All of these samples have low Nb/Y ratios (0.04–0.19), similar to those of N-MORBs recovered from the east subbasin of the SCS (0.08–0.14) at Integrated Ocean Drilling Program (IODP) Site U1431 (Figure 1a; G. L. Zhang et al., 2018), and they plot in the subalkaline basalt field on the Zr/TiO_2-Nb/Y diagram (Figure 5b). The N-MORB-type samples exhibit wide variations in their major element concentrations, for example, their SiO_2 contents range from 49.10 to 56.12 wt.%, their MgO contents range from 3.76 to 12.25 wt.%, their Al_2O_3 contents range from 12.92 to 25.67 wt.%, their TiO_2 contents range from 0.26 to 1.94 wt.%, and their P_2O_5 contents range from 0.01 to 0.26 wt.%.

The ΣREE (total rare earth element, REE) contents of the N-MORB-type samples range from 6.62 to 66.03 ppm, with an average value of 32.37 ppm (Table S1), which are similar to those of the N-MORBs from Site U1431 (ΣREE = 28.10–46.37 ppm, average 36.35 ppm; G. L. Zhang et al., 2018). The N-MORB types display concordant light rare earth element (LREE)-depleted chondrite-normalized patterns (Figure 6a) parallel to the average N-MORB pattern (Sun & McDonough, 1989), thus distinguishing them from OIB and E-MORB, which are LREE-enriched relative to heavy rare earth elements (HREEs) and exemplified by ΣLREE/ΣHREE = 1.07–1.86, $(La/Yb)_N$ = 0.45–1.18 and $(La/Sm)_N$ = 0.48–1.01. These compositions are similar to those of the N-MORBs (ΣLREE/ΣHREE = 1.25–1.56, $(La/Yb)_N$ = 0.57–0.87, $(La/Sm)_N$ = 0.53–0.75) recovered at IODP Site U1431 in the SCS (G. L. Zhang et al., 2018). The nearly flat HREE patterns represent melts that formed at <90 km in the asthenosphere, that is, above the garnet-peridotite stability field (Said & Kerrich, 2009). No significant Ce anomalies (δCe = 0.96–1.09) are observed in these samples, while their Eu

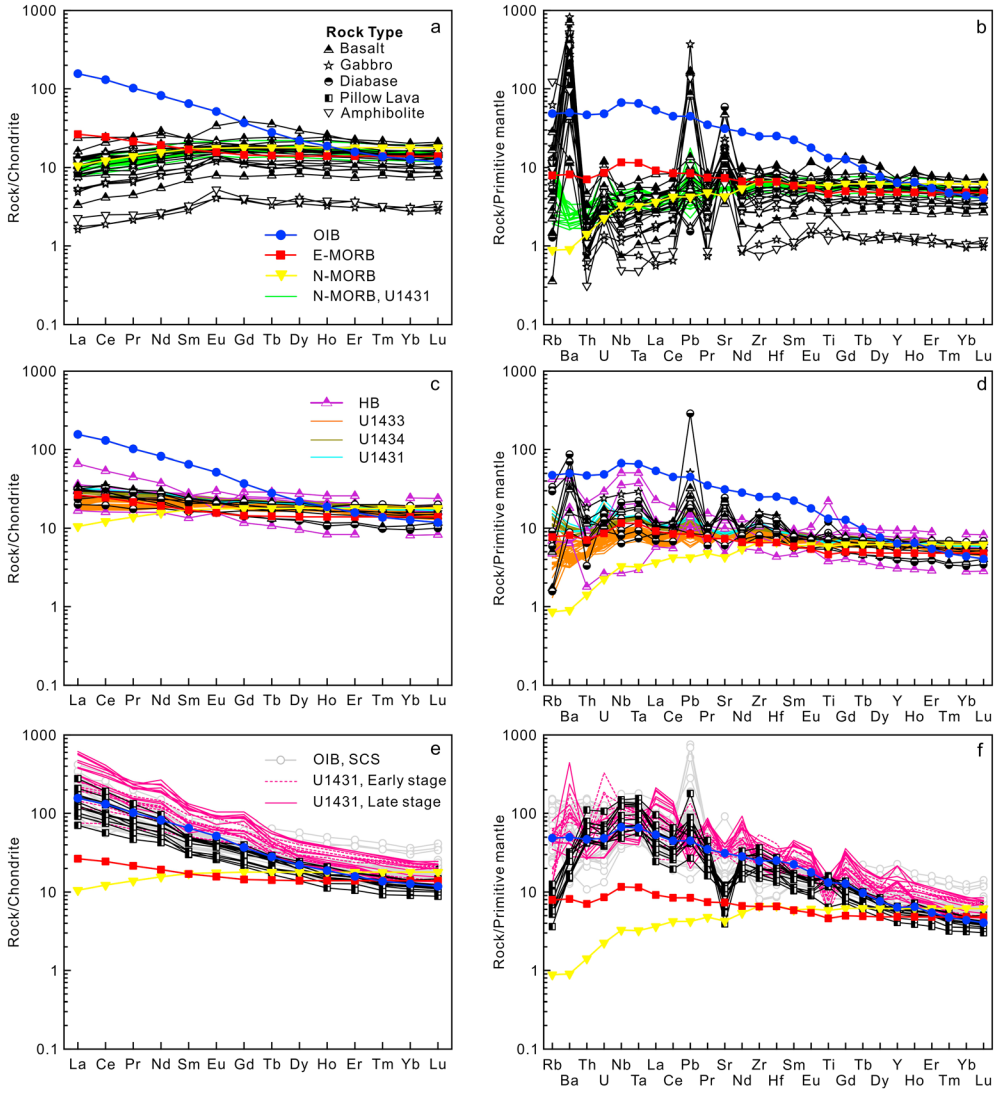

Figure 6. Chrondrite-normalized REE patterns and primitive mantle-normalized trace element diagrams for N-MORB types (a, b), E-MORB types (c, d), and OIB types (e, f). Modern N-MORB, E-MORB, OIB, and normalization values are from Sun and McDonough (1989). Huatung Basin data are from Hickey-Vargas et al. (2008). Data for OIB-like seamount basalts in the SCS are from Yan et al. (2015, 2008). Data for samples recovered from the SCS at Integrated Ocean Drilling Program sites are from G. L. Zhang et al. (2018, 2017). SCS = South China Sea; N-MORB = normal mid-ocean ridge basalt E-MORB = enriched mid-ocean ridge basalt; OIB = ocean island basalt.

anomalies vary greatly (δEu = 0.90–1.49), indicating that different degrees of plagioclase fractionation occurred during the generation and evolution of these magmas (Saccani et al., 2014).

On the primitive mantle-normalized multielement variation diagram (Figure 6b), samples with N-MORB affinity display U enrichment decoupled from Th, which may be ascribed to the partitioning of the excess U in seawater into basalts during seafloor hydrothermal alteration (Khogenkumar et al., 2016; MacDougall et al., 1979). Most of the N-MORB-type samples exhibit enrichment in Rb, Ba, Pb, and Sr, while several others show depletion, thus reflecting the mobility of LILEs. The low contents of HFSEs and left dipping trend of Nb-Ta-La-Ce are consistent with a depleted mantle source (G. Yang et al., 2012). The elements from Nd to Lu show a generally flat pattern, which is indicative of oceanic basalt (Pearce, 1983). All of these trends are similar to those of the average N-MORB (Sun & McDonough, 1989) and the N-MORBs from the SCS (G. L. Zhang et al., 2018). The N-MORB types also have trace element ratios (Zr/Nb = 14.13–47.61, Zr/Hf = 25.71–40.54, Nb/Ta = 10.04–17.73) that resemble those of typical N-MORB (~30, ~36, and 6–14, respectively; Rollinson, 1993). The geochemical signature of the N-MORB-type rocks, particularly their

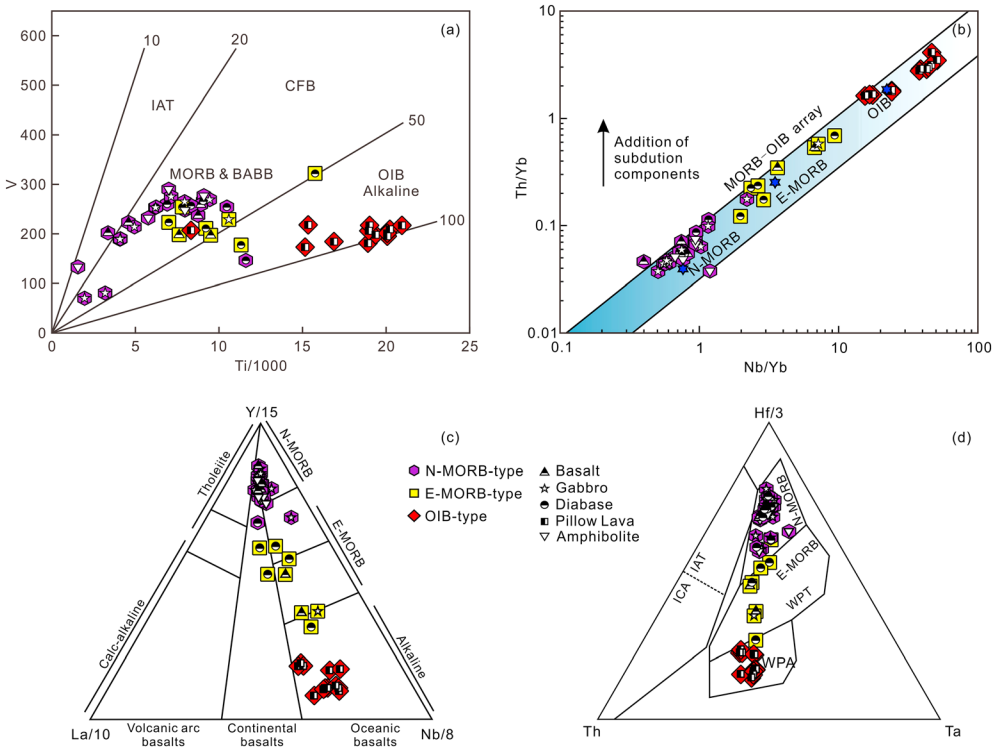

Figure 7. Tectonic discrimination diagrams for the igneous rocks from the Hengchun Peninsula. (a) V-Ti/1000 diagram (Shervais, 1982); (b) Th/Yb versus Nb/Yb diagram (the field of the MORB-OIB mantle array is from Pearce, 2008); (c) Y/15-La/10-Nb/8 diagram (Cabanis & Lecolle, 1989); and (d) Th-Ta-Hf/3 diagram (Wood, 1980). Abbreviations: MORB = mid-oceanic ridge basalt; BABB = back-arc basin basalt; IAT = island arc tholeiite; CFB = continental flood basalt; WPT = within plate tholeiite; WPA = within plate alkali basalt; ICA = island arc calc-alkaline basalt; OIB = ocean island basalt.

Ti/V ratio, is typical of MORB or back-arc basin basalt (BABB; Figure 7a). On the Th/Yb versus Nb/Yb diagram (Figure 7b), most of the N-MORBs show elemental ratios approximately the same as that of the averaged N-MORB defined by Sun and McDonough (1989). In Figure 7d, the N-MORB-type samples cluster in the field of N-MORB compositions. Therefore, they were most likely derived from a depleted mantle source. Meanwhile, some N-MORB types exhibit weakly negative Nb and Ta (and Ti) anomalies (Figure 6b) and trend toward the continental basalt field on the Y/15-La/10-Nb/8 diagram (Figure 7c; Cabanis & Lecolle, 1989), thus showing an affinity to BABB. The Cr and Ni concentrations (Cr = 175–370 ppm and Ni = 58.7–138 ppm) of these samples are lower than those of primitive basaltic magma (Cr = 300–500 ppm and Ni = 300–400 ppm; Tatsumi & Ishizaka, 1981), with Ni/Cr ratios of less than 0.6, implying that fractional crystallization of olivine has occurred.

5.2.2. E-MORB Type

The E-MORB-type samples are represented by rocks from the Jianshan area (Figure 3a), including gabbros, diabases, and basalts with the following major element contents: 48.83–56.73 wt.% for SiO_2, 4.24–8.92 wt.% for MgO, 14.53–18.56 wt.% for Al_2O_3, 1.17–2.83 wt.% for TiO_2, and 0.13–0.28 wt.% for P_2O_5. The E-MORB-type rocks exhibit a compositional transition from subalkaline to alkaline (Figure 5b), with Nb/Y ratios ranging from 0.19 to 0.84; they thus resemble the basaltic rocks from the Huatung Basin (Nb/Y = 0.14–1.14; Hickey-Vargas et al., 2008). In contrast, the E-MORBs from the SCS (IODP Site U1431 in the east subbasin, Nb/Y ~ 0.33; Sites U1433 and U1434 in the Southwest subbasin, Nb/Y = 0.16–0.29) are all alkaline (Figure 1a; G. L. Zhang et al., 2018). The chondrite-normalized REE patterns of the E-MORB-type rocks are shown in Figure 6c and compared with those of the E-MORB-like rocks from the Huatung Basin (Hickey-Vargas et al., 2008) and the SCS (G. L. Zhang et al., 2018). The E-MORB-type rocks within the Hengchun accretionary prism exhibit REE patterns that are transitional between those of N-MORB and OIB (ΣLREE/ΣHREE = 1.97–3.64, $(La/Sm)_N$ = 1.05–1.92, $(La/Yb)_N$ = 1.22–3.37). They display a remarkable geochemical variation similar to that of rocks from the Huatung Basin (ΣLREE/ΣHREE = 1.58–4.04, (La/

Sm)$_N$ = 1.11–2.46, (La/Yb)$_N$ = 1.07–3.98). Contrastively, REE patterns of the E-MORBs from the SCS are relatively consistent and well confined ((ΣLREE/ΣHREE ≈ 2.61, (La/Sm)$_N$ ≈ 1.32, (La/Yb)$_N$ ≈ 1.87) for E-MORBs from the east subbasin; and (ΣLREE/ΣHREE = 1.91–2.36, (La/Sm)$_N$ = 0.82–1.18, (La/Yb)$_N$ = 1.01–1.73) for E-MORBs from the southwest subbasin).

The E-MORB-type samples display primitive mantle-normalized multielement patterns with great variations, which are similar to those of the E-MORBs from the Huatung Basin and distinct from those from the SCS (Figure 6d). They are generally enriched in LILEs (e.g., Rb, Ba, Pb, and Sr) and some HFSEs (e.g., Nb, Ta, Zr, and Hf). As oceanic lithosphere is subducted within a convergent margin, Th and LREE are released from the subducted oceanic lithosphere to the overriding mantle wedge, whereas Nb is preserved in the residual slabs. Therefore, although arc magmas are characterized by LREE enrichment, they also have negative Nb anomalies (Saunders et al., 1996). However, in the E-MORB-type samples exhibiting decoupled contents of Th and U, no negative Nb anomalies were observed (Nb/Th > 8, 10.49–16.42). There are also no obvious Eu or Ce anomalies in these samples (δEu = 0.93–1.07, δCe = 1.00–1.11). The E-MORB-type samples have moderate V/Ti, Th/Yb and Nb/Yb ratios and plot in the transition zone between N-MORB and OIB (Figures 7a–7d). In summary, these E-MORB-type rocks were derived from a depleted MORB mantle (DMM) metasomatized by an enriched endmember to some extent, rather than representing the products of a subduction system.

5.2.3. OIB Types

The samples with OIB affinity are alkaline basalts (Figure 5b) collected from the Ssuchungchi Gorge and Liangluanxi areas (Figure 3a). Their major element contents are described as follows: 46.36–53.56 wt.% SiO_2, 3.88–8.88 wt.% MgO, 15.00–18.48 wt.% Al_2O_3, 1.39–3.50 wt.% TiO_2, and 0.12–0.97 wt.% P_2O_5. The ΣREE contents of the OIB-type samples (98.18–269.33 ppm, average 169.61 ppm) are generally lower than those of typical OIB (198.9 ppm; Sun & McDonough, 1989) and mostly fall in the range of alkaline OIB-type seamount basalts from the SCS (112.17–429.19 ppm, average 215.98 ppm; Yan et al., 2015, 2008).

The chondrite-normalized REE patterns of all OIB-type samples exhibit pronounced enrichment in LREE relative to HREE (Figure 6e), which is corroborated by their values of ΣLREE/ΣHREE = 5.16–13.03, (La/Yb)$_N$ = 6.12–20.64, and (La/Sm)$_N$ = 2.33–5.57, which are in good accordance with those of OIBs from the SCS (ΣLREE/ΣHREE = 3.92–14.02, (La/Yb)$_N$ = 4.49–23.90 and (La/Sm)$_N$ = 1.75–5.77;Yan et al., 2015, 2008). These low HREE contents suggest that the primitive magma for these alkaline OIBs may have been generated at deep levels, where the residual phases are dominated by garnets or titanites instead of plagioclase (G. Yang et al., 2012). No obvious Ce or Eu anomalies (δCe = 0.93–1.03 and δEu = 0.96–1.06) were observed, indicating that a negligible quantity of plagioclase was retained in the residue after the partial melting of the source mantle or was fractionated from the melt during its ascent and emplacement.

The alkaline OIBs within the Hengchun accretionary prism exhibit strong covariation in the primitive mantle-normalized multielement diagram (Figure 6f) and are uniformly depleted in Rb, Ba, and Sr but enriched in Pb. The OIB-type samples show obvious positive Nb and Ta anomalies, similar to the OIBs from the seamounts in the SCS (Yan et al., 2015, 2008) and the late-stage volcanic clasts recovered at IODP Site U1431 (G. L. Zhang et al., 2017), which also show OIB affinity. The alkaline OIBs within the prism have high contents of HFSEs relative to MORB and exhibit a progressive decrease from Th to Lu (except for Pb and Sr) in the multielement variation diagram (Figure 6f), which is indicative of intraplate basaltic rocks derived from a geochemically enriched mantle source. This interpretation is corroborated by the high Ti/V, Th/Yb, and Nb/Yb ratios (Figures 7a and 7b) of these samples and by the projection of the OIB-type samples on the tectonic discrimination diagrams (Figures 7c and 7d).

5.3. Zircon U-Pb Geochronology

Both the amphibolite samples KT-21 and SG-06 chosen for zircon U-Pb dating are of N-MORB affinity. Their analytical data and calculated ages are shown in Table S2.

The zircon grains from KT-21 are generally colorless and transparent. These grains are mainly subhedral to euhedral, equant to long prismatic, and feature sharp or rounded terminations in their morphology. The lengths of the zircon grains range from 80 to 150 μm, and their length/width ratios vary between 1:1 and 3:1. Their CL images (Figure 8a) illustrate that all zircon grains have distinct oscillatory zoning without visible inherited cores. Eighteen analytical spots from sample KT21 yielded a wide range of U (30–557 ppm) and

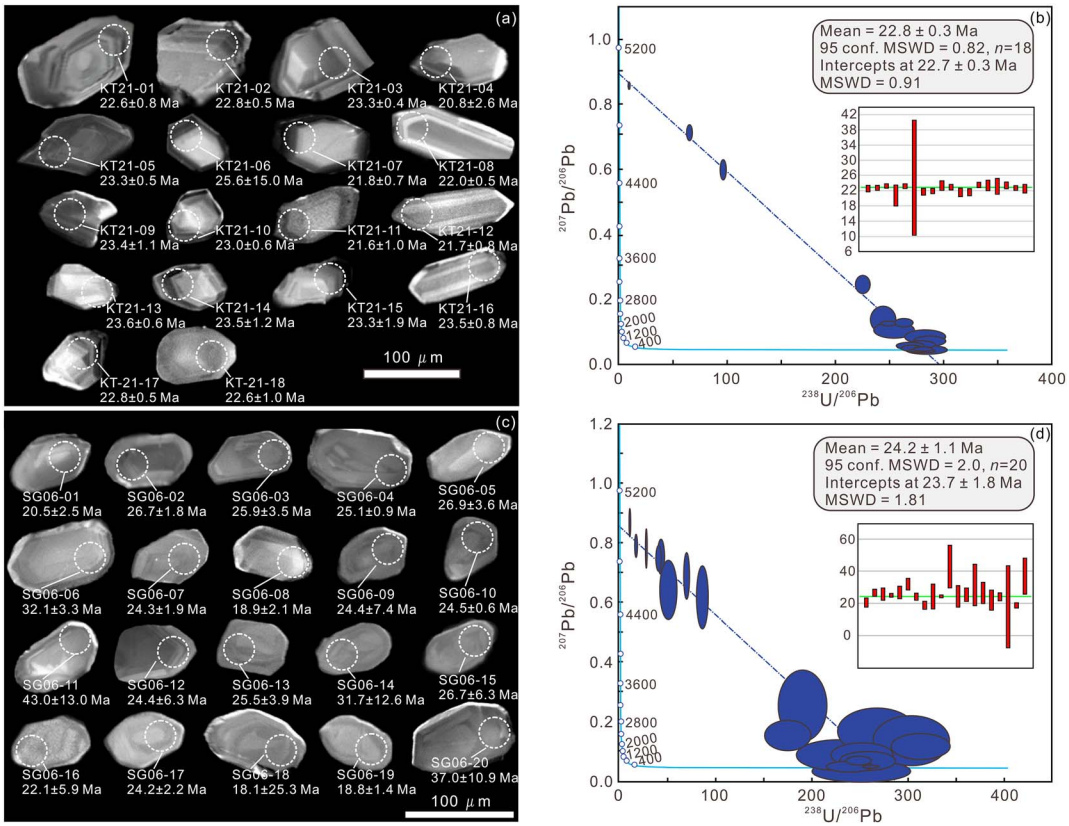

Figure 8. Cathodoluminescence images and U-Pb Tera-Wasserburg inverse concordia diagrams for zircons in amphibolite samples KT21 (a and b) and SG06 (c and d).

Th (7–315 ppm) concentrations, with Th/U ratios ranging from 0.214 to 1.160 (Table S2). In comparison with metamorphic zircons, whose Th/U ratios are mostly less than 0.1 (Rubatto, 2002), the zircons from KT-21 show features indicative of their magmatic origin, which is also corroborated by their characteristic oscillatory zoning (Hartmann & Santos, 2004).

Because the error correlation between $^{207}Pb/^{206}Pb$ and $^{238}U/^{206}Pb$ is weaker than that between $^{206}Pb/^{238}U$ and $^{207}Pb/^{235}U$, the Tera-Wasserburg diagram (Tera & Wasserburg, 1972), known as the inverse concordia diagram, was used to evaluate the analytical results (Corfu, 2013; Hosseini et al., 2017). Moreover, zircons younger than 200 Ma are usually characterized by high common Pb/radiogenic Pb ratios, as corroborated by their correlated arrays to high $^{207}Pb/^{206}Pb$ ratios on the Tera-Wasserburg diagram (Williams, 1998). The analytical data define a linear regression on the Tera-Wasserburg diagram (Figure 8b), demonstrating the existence of common Pb. The regression of the analyses yielded a lower intercept age at 22.86 ± 0.32 Ma (MSWD = 0.91) and a *Y* intercept of the $^{207}Pb/^{206}Pb$ ratio at 0.8957 (Figure 8b), which was used for the ^{207}Pb-based common Pb correction (Jiang et al., 2018). The ^{207}Pb-based common Pb-corrected $^{206}Pb/^{238}U$ ages range from 20.80 to 25.60 Ma. The weighted mean ^{207}Pb-corrected $^{206}Pb/^{238}U$ age obtained for KT21 is 22.8 ± 0.3 Ma (n = 18, 2σ, MSWD = 0.82).

The zircon grains separated from SG-06 are transparent and colorless and occur as stubby to prismatic crystals that are generally 70–100 μm long, with aspect ratios ranging from 4:3 to 2:1. The CL images exhibit blurred oscillatory or lath-shaped zoning without visible inherited cores (Figure 8c). Twenty zircon grains were analyzed, and the results (Table S2) show a wide range of Th (5–224 ppm) and U (1–46 ppm) contents, with Th/U values of >0.1 (0.136–0.444), thus implying that they have a magmatic origin. All 20 analyses define a linear array on the Tera-Wasserburg diagram (Figure 8d), with a lower intercept age at 23.7 ± 1.8 Ma (MSWD = 1.81) and a *Y* intercept of the $^{207}Pb/^{206}Pb$ ratio at 0.8570. The ^{207}Pb-based common Pb correction was conducted based on this value, yielding common Pb-corrected $^{206}Pb/^{238}U$ ages varying

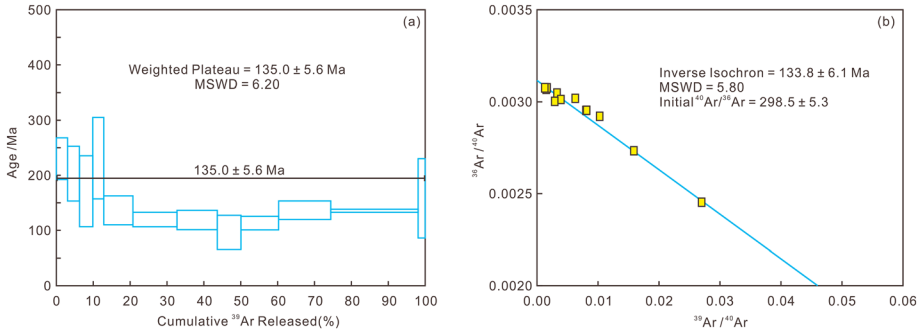

Figure 9. ^{40}Ar/^{39}Ar age plateau and inverse isochron of plagioclase from gabbro sample SG08.

between 18.1 Ma and 43.0 Ma. All of these analyses yielded a weighted mean age of 24.2 ± 1.1 Ma for SG-06 (MSWD = 1.81; Figure 8d).

5.4. ^{40}Ar/^{39}Ar Dating

The E-MORB-type gabbro sample SG08 from the Ssuchungchi Gorge was chosen for ^{40}Ar/^{39}Ar dating. A total of 12 incremental heating steps was carried out with temperatures ranging from 830 to 1400 °C to provide more details about the outgassing behavior of the sample. The result of the ^{40}Ar/^{39}Ar analysis is presented in Table S3, and the corresponding plateau age and inverse isochron age are shown in Figure 9. The sample yielded a more or less flat spectrum that did not show a loss of ^{40}Ar* from the lowest-temperature steps. The spectra show older apparent ages at lower-temperature steps (<960 °C, Table S3), which can be attributed to the effects of recoil loss or the redistribution of argon isotopes (Foland et al., 1984; Turner & Cadogan, 1974). Despite the large errors of the apparent ages, which can be attributed to the low K content in the mineral analyzed here, the sample yielded ^{40}Ar/^{39}Ar plateau and isochron ages of 135.0 ± 5.6 Ma (MSWD = 6.20) and 133.8 ± 6.1 Ma (MSWD = 5.80), respectively. The radiogenic component of sample SG8 intercepting the *X* axis corresponds to ^{40}Ar*/^{39}Ar$_k$ = 21.95. The contamination component, that is, the *Y* intercept, suggests an initial ^{40}Ar/^{36}Ar ratio (298.5 ± 5.3; Figure 9b) that is approximately the same as the atmospheric value (295.5 ± 0.5), thus indicating the age obtained here is reliable.

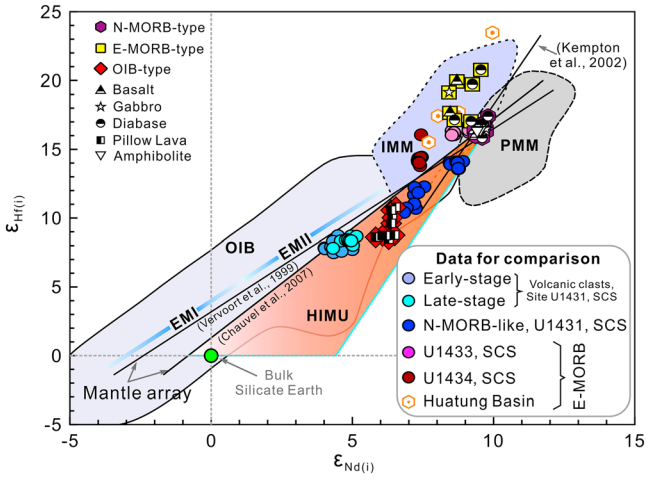

Figure 10. Plot of initial ε_{Nd}-ε_{Hf} data after Kempton et al. (2002) for the accreted mafic rocks from the Hengchun Peninsula, compared with basalts from the Huatung Basin (Hickey-Vargas et al., 2008) and the South China Sea (G. L. Zhang et al., 2018, 2017). See additional supporting information Data Set S1 for data sources. IMM = Indian MORB source mantle; PMM = Pacific MORB source mantle. The IMM and PMM discriminant boundary is proposed by Kempton et al. (2002). The mantle arrays are defined by Vervoort et al. (1999) and Chauvel et al. (2007). The ranges of EMI and EMII (EM: enriched mantle), are from Niu and O'Hara (2003). The high-μ field is from Wang et al. (2014).

5.5. Hf-Nd Isotopic Compositions

Hf-Nd isotopic compositions are considered to be retained during subduction processes and are favorable for distinguishing mantle sources in convergent boundary settings (Kempton et al., 2002; Pearce et al., 2007). The analytical results of the Hf-Nd isotopic analyses of 29 samples of the accreted mafic rocks from the Hengchun Peninsula are shown in Table S4 and displayed on the isotopic correlation diagram in Figure 10.

N-MORB-type samples have high ^{143}Nd/^{144}Nd and ^{176}Hf/^{177}Hf ratios that cluster in relatively limited ranges of 0.513117–0.513145 and 0.283216–0.283262, respectively, indicating that they were derived from a single homogeneous mantle source similar to DMM. Based on the ages obtained in this study, the Hf-Nd isotopic compositions of the N-MORB-type samples are corrected to 24 Ma (Table S4). The Nd and Hf isotopic compositions of all N-MORB types are well correlated, plotting along the mantle array (Chauvel et al., 2007; Vervoort et al., 1999) and in the overlapping field of Indian MORB mantle (IMM) and Pacific MORB mantle on the εNd-εHf diagram (Figure 10).

The Nd isotopic compositions (^{143}Nd/^{144}Nd = 0.512929–0.512967, εNd = 5.66–6.42) of the alkaline OIBs from the Hengchun Peninsula are similar to those of the Daimao seamount basalts (^{143}Nd/^{144}Nd = 0.512957–0.512967 and εNd = 6.22–6.42) from the SCS (Yan et al.,

2015). Based on the geochemical similarity between the OIB-type samples and the Daimao seamount (16.5 Ma), as well as the age of the Shihmen Conglomerate (middle Miocene), their isotopic compositions are corrected to an assumed age of 15 Ma (Table S4). The OIB-type samples have systematically lower $^{176}Hf/^{177}Hf$ values ($^{176}Hf/^{177}Hf$ = 0.283004–0.283070 and εHf = 8.19–10.53) at a given $^{143}Nd/^{144}Nd$ value, which are clearly distinguishable from the global mantle array (Figure 10) and plot in the HIMU (high-μ, $\mu = {}^{238}U/^{204}Pb$) field defined by Wang et al. (2014), indicating that their mantle source is substantially a binary mixing of DMM-EMII and influenced by a HIMU-like mantle component at different extent (Nebel et al., 2013; Salters & White, 1998).

The E-MORB-type samples are characterized by Nd-Hf decoupling, with an apparently large variation in radiogenic Hf isotopic composition ($^{176}Hf/^{177}Hf$ = 0.283214–0.283315 and εHf = 15.65–19.22) at a given Nd isotopic composition ($^{143}Nd/^{144}Nd$ = 0.513034–0.513100 and εNd = 7.73–9.02). The Hf isotopes of the E-MORBs recovered from the SCS ($^{176}Hf/^{177}Hf$ = 0.283158–0.283242 and εHf = 13.20–16.16; G. L. Zhang et al., 2018) are less radiogenic than those of the E-MORB-type samples within the Hengchun accretionary prism (Figure 10). Based on the $^{40}Ar/^{39}Ar$ age obtained in this study, the Hf-Nd isotopes are corrected to an age of 135 Ma (Table S4). On the εNd-εHf diagram (Figure 10), all the E-MORB-type samples deviate from the mantle array and plot in the IMM field, together with the basalts from the Huatung Basin (Hickey-Vargas et al., 2008).

6. Discussion

6.1. Provenances of the Accreted Mafic Rocks

Based on the associated microfossils within the turbiditic sequences of the Hengchun accretionary prism, Muller et al. (1984) proposed that the accreted basalts were late Oligocene to early Miocene in age (18–24 Ma). The amphibolites from the Kenting Mélange yielded early Miocene K-Ar hornblende ages of 22–23 Ma (Pelletier & Stephan, 1986) and a late Oligocene U-Pb zircon age of ~25 Ma (X. C. Zhang et al., 2016). The U-Pb age spectra of the detrital zircon grains in the Shihmen Conglomerate exhibit a peak between 20 and 25 Ma (Tsai & Shyu, 2015). All of these geochronological results are consistent with the zircon U-Pb ages of the N-MORB-type samples obtained in this study, and all of them correlate to the seafloor spreading period of the SCS (33–15 Ma; Briais et al., 1993; L. Chen et al., 2017; Hernandez Almeida, 2014; X. H. Li et al., 2014; Taylor & Hayes, 1983). The N-MORB-type samples have similar geochemical compositions as the N-MORBs drilled from the SCS. The negative Nb anomalies of BABB rocks are generally attributed to the influx of subduction components into a depleted mantle source (Pearce & Stern, 2006). Thus, the BABB affinity shown by some N-MORB-type samples (Figure 6b) can be ascribed to the metasomatism of the DMM-like mantle caused by the subduction of the Paleo-Pacific Plate beneath the Eurasian continent during the late Mesozoic, which resulted in the formation of the SCS (Taylor & Hayes, 1983; Yu et al., 2018). Additionally, the uniform Hf-Nd isotopes of the N-MORBs are indicative of a single homogeneous DMM-like source. Accordingly, we conclude that the N-MORB-type rocks, which are dominant among the accreted mafic rocks, represent the debris of the subducted oceanic crust of the SCS.

Voluminous OIB-type intraplate volcanic rocks derived from the passive upwelling of enriched asthenosphere due to continental rifting were erupted on the South China continental margin since the late Paleocene (X. L. Huang et al., 2013; Yu et al., 2018). However, the geochemical compositions of the alkaline OIBs in this study reflect no influence of continental contamination, for example, their Nb/Ta ratios (14.84–18.22, average 16.80) are close to those of the primitive mantle (Nb/Ta = 17.59; Hofmann, 1988) and obviously higher than those of continental crust (Nb/Ta = 11.43; Rudnick & Gao, 2003). Additionally, the well-preserved pillow structures in the massive OIB blocks are indicative of a submarine eruption environment. The SCS underwent three episodes of seafloor spreading: Seafloor spreading commenced in the East and NW subbasins at 33 and ~30 Ma, respectively. And then, right after the ridge jump in the East subbasin (~23.5 Ma), spreading started in the SW subbasin (Yan et al., 2015; Yu et al., 2018). A series of seamounts, with ages of 3.49–18.61 Ma, generally formed along the fossil ridges ~6–12 Ma after the cessation of each spreading stage (Figure 1a; Wang et al., 1985; Yan et al., 2015, 2014, 2008). Geochemical analyses reveal that the mantle source of the alkaline OIBs from these seamounts was generated by mixing between DMM and EMII (possibly the Hainan plume), along with an endogenous Dupal mantle component beneath the SCS (Yan et al., 2015, 2008). The OIB types from the Hengchun Peninsula display uniform chondrite-

normalized REE patterns and primitive mantle-normalized incompatible trace element patterns (Figures 6e and 6f), suggesting that they originated from the same geologic setting. In addition, all alkaline OIBs exhibit apparent geochemical similarities with the seamount basalts from the SCS. Therefore, in contrast to the ambiguous origins (the West Philippine Sea and/or the SCS) proposed by H. Y. Chen et al. (2018), we conclude that all the OIBs within the Hengchun accretionary prism represent the products of the postspreading intraplate magmatism in the SCS.

The E-MORB-type samples show geochemical and Hf-Nd isotopic compositions that are distinct from those of the E-MORBs recovered from the SCS, for example, greater geochemical variation and more radiogenic Hf isotopes at a given Nd isotopic composition (Figure 10), indicating that they were not scraped off from the subducted SCS lithosphere. Based on the detrital zircon U-Pb geochronology of the sandstones and the Nd isotopic compositions of the mudstone interlayers in the turbidite sequences in the Hengchun Peninsula, X. C. Zhang et al. (2014) and Tsai (2017) argued that all sedimentary materials are derived from the SCS and no components from the volcanic arc are involved. However, the basaltic rocks from the overriding plate cannot necessarily be excluded. Based on Pb isotope analysis, H. Y. Chen et al. (2018) proposed that all of the accreted E-MORB-type rocks originated from the West Philippine Basin. However, the Pb isotopic compositions of the accreted rocks may have been distorted during alteration and are therefore likely to be equivocal. More importantly, the Gagua Ridge, which is located between the Huatung Basin and the West Philippine Basin (Figure 1) and was uplifted long before the opening and subduction of the SCS, could have blocked any components from the West Philippine Basin from entering the Hengchun accretionary wedge. The E-MORB-type samples yield an early Cretaceous age of ~135 Ma and exhibit geochemical characteristics similar to those of basalts from the Huatung Basin (Deschamps et al., 2000; Hickey-Vargas et al., 2008), which also exhibit distinct geochemical variations and a pronounced IMM-type Hf-Nd isotopic signature (Figure 10). Therefore, the E-MORBs that accreted in the prism are most likely fragments of the Luzon forearc, rather than rocks from the SCS or the West Philippine Basin to the east of the Gagua Ridge.

6.2. Mantle Evolution of the SCS

N-MORB-like basalts and volcanic clasts have been recovered from the SCS at IODP Site U1431 (Figure 1a). The early-stage volcanic clasts are obviously carbonated, enriched in LREEs and depleted in Nb and Ta, while the late-stage clasts have less enriched LREE contents and positive Nb-Ta anomalies similar to typical alkaline OIBs (G. L. Zhang et al., 2018, 2017). G. L. Zhang et al. (2017) proposed that the carbonated silicate melts, which are most likely derived from carbonated eclogite produced by oceanic crust recycling, were converted to alkaline basaltic melts through reactions with the lithospheric mantle. During such reactions, dissolution of orthopyroxene from the country rock introduced geochemically depleted components into the melts, while precipitation of apatite accounts for reduction of LREEs and genesis of positive Nb-Ta anomalies. All these samples plot below the mantle array in Figure 10, implying the influence of a HIMU-like mantle component (Nebel et al., 2013), which is believed to be related with recycled oceanic crust (Chauvel et al., 2007; Nebel et al., 2013; Salters & White, 1998) and the metasomatism of carbonated melt (Collerson et al., 2010; Dasgupta et al., 2007). The alkaline OIBs accreted in the Hengchun accretionary prism have similar geochemical compositions with the late-stage clasts, for example, relatively low MgO contents among global OIBs (<10%, Table S1), enriched LREE contents, negative Y anomalies (Y/Y^{*} = 0.74–1.03), positive Nb-Ta anomalies (Figure 6f) and HIMU-type Hf-Nd isotopic signatures (Figure 10), thus indicating their genetic connections.

On the εNd-εHf diagram (Figure 10), the alkaline OIBs from the Hengchun Peninsula define a trend below the mantle array that curves inward to the OIB field with radiogenic Nd together with the rocks collected from IODP Site U1431 in the SCS, similar to the case of the Cook-Austral island chain in the South Pacific (Salters et al., 2011), indicating the existence of at least three components in this suite: DMM, HIMU, and EMII. The N-MORBs within the Hengchun accretionary prism are less influenced by enriched components compared with the N-MORB-like basalts from the fossil ridge of the SCS (Site U1431; G. L. Zhang et al., 2018), because the latter represents the final products of the spreading ridge and was formed spatially and temporally close to the emplacement of postspreading magmatism (seamounts). Most likely, the N-MORB types within the Hengchun accretionary prism were less/not affected by the EMII-related Hainan Plume (Yan et al., 2018, 2008), which upwelled the recycled oceanic crustal components from the

deep mantle and interacted with the lithospheric mantle, resulting in carbonated silicate melts (G. L. Zhang et al., 2017) and OIBs with HIMU-type Hf-Nd isotopic signatures in the SCS.

6.3. Tectonic Implications in the Northern Manila Subduction Zone

As described above, all of the N-MORB-type basalts within the Hengchun accretionary wedge were off-scraped from the subducted oceanic crust of the SCS together with the overlying fine-grained sediments derived from the South China continent (Kirstein et al., 2010; X. C. Zhang et al., 2014). This can be attributed to the volumetric prevalence of N-MORB in the oceanic crust (H. Y. Chen et al., 2018) and is a normal phenomenon in accretionary complexes. In contrast, the OIBs and E-MORBs, which show geochemical signatures resembling those of seamount basalts from the SCS and mafic rocks from the Huatung Basin, respectively, are highly indicative of the tectonic evolution of the northern Manila subduction zone.

Regardless of the cause of seamounts on the seafloor, they are carried along by plate movements and will ultimately be subducted into the deep mantle or accreted onto accretionary prisms (G. Yang et al., 2015). Isolated OIB blocks within onshore accretionary prisms are usually considered accreted seamount fragments (Isozaki et al., 1990; G. Yang et al., 2015). They are interpreted as faulted fragments that were structurally incorporated into the accretionary prism during seamount subduction (Okamura, 1991; Ueda et al., 2002) or sedimentary blocks due to the gravity-driven collapse of seamounts at the trench (Sano & Kanmero, 1991). Seismic surveys have revealed that appreciable amounts of volcanics with high magnetization have been subducted, at least, beneath the lower-slope domain and that volcanic seamounts buried beneath the incoming sediments are about to be subducted or accreted onto an accretionary prism (Hsu et al., 2004; A. T. Lin et al., 2009). Additionally, some of the alkaline pillow lavas with OIB affinity in the Liangluanxi area are intensively sheared and fractured, implying the influence of accretion-related deformation. Folds and shear joints are extraordinarily developed in the adjacent sedimentary rocks (Mutan Formation). Therefore, the OIBs in the Hengchun accretionary prism, especially those appear as massive angular blocks or with well-preserved pillow structures, are indicative of seamount subduction in southern Taiwan.

The consumption of the Luzon forearc east of Taiwan is gradually enhanced northward (Figure 11a), which is not consistent with typical arc-continent collision models (Cheng, 2009; Liu et al., 1992; Malavieille et al., 2002; Malavieille & Trullenque, 2009; Meschede, 2014; Shyu et al., 2011). Physical and numerical models have proposed that two or three forearc slices are continuously subducting eastward along an east dipping thrust fault into the mantle beneath the Huatung Basin and that abundant forearc fragments are buried in the upper to middle crust beneath the Central Range (Cheng, 2009; Malavieille et al., 2002). As shown in Figure 1b, the Huatung-Philippine Sea Plate simultaneously participates in the northern Manila and Ryukyu subduction systems, which are mutually perpendicular, acting as the overriding and subducting plate respectively. As a result, there is a strike-slip component in the relative movement between the SCS and Huatung-Philippine Sea Plates. There are two possible geodynamic mechanisms for the entrance of forearc fragments (E-MORBs) into the accretionary complex: Most likely, they originated from the frontal prism (Vannucchi et al., 2012; Von Huene et al., 2004), which comprises forearc fragments that have been laterally transported by strike-slip movement between converging plates (Beck, 1983, 1986). These forearc materials may have been snatched from the overriding plate due to the tectonic erosion caused by excessive shear stress between the converging plates, as the younger, and thereby intrinsically more buoyant, oceanic crust of the SCS subducted beneath the older and presumably denser Huatung Basin (Shao et al., 2015). Alternatively, these materials may have been off-scraped from the subducted Luzon forearc slices.

6.4. Tectonosedimentary Model

According to their lithology, geochemistry, and geochronology, all of the diverse igneous rocks within the Hengchun accretionary prism are basaltic fragments from both the subducting and overriding plates, and no granitic or basaltic rocks from the South China continental margin have been recognized. Therefore, the hypothesis that the igneous pebbles within the turbidite sequences were rounded and accumulated in a submarine channel on the passive Eurasian continental margin before being accreted into the Hengchun accretionary prism in the Late Miocene is logically flawed. A more plausible explanation is that the accreted mafic rocks were recycled and rounded during the temporary emergence and exhumation of the accretionary prism. The subduction of a seamount or a seamount chain, which is a very short tectonic event, can dramatically impact the tectonics in a subduction zone. It causes the abrupt uplift and significant

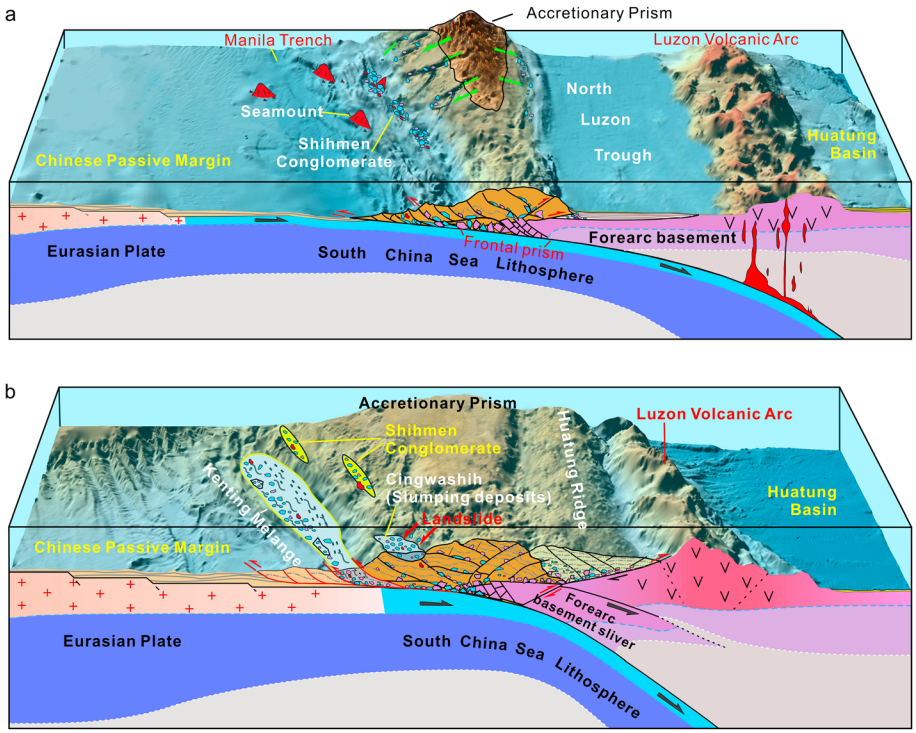

Figure 11. Tectonic evolution and tectonosedimentary model in southern Taiwan: (a) Temporary sediment recycling caused by seamount subduction, resulting in the sporadic embedding of the Shihmen Conglomerate in the turbidite sequences. (b) Formation of the Kenting Mélange due to continental subduction and arc-continent collision.

transfer of internal material within the accretionary wedge, the subsequent subsidence and collapse of the inner trench slope, and changes in the subduction channel and complex faults as candidates for mélange genesis (Dominguez et al., 2000; Okamura, 1991; Von Huene et al., 2000; G. Yang et al., 2015). The presence of alkaline OIBs, especially the isolated massive pillow lava blocks within the Shihmen Conglomerate (Figure 3f), implies that the sporadically distributed Shihmen Conglomerate may be resulted from seamount subduction.

The Shihmen Conglomerate is composed of several gravel layers; each of them are several tens of meters thick, grading upward from pebbles of 1–15 cm in diameter to sandstone layers alternating with siltstones. Some of the sandstone stratum are covered by carbonates a few centimeters thick (Pelletier & Stephan, 1986). Additionally, the fossil fragments of oyster and conch in the Shihmen Conglomerate (not shown) and the well-preserved oyster and leaf fossils in the Lilungshan Formation (X. C. Zhang et al., 2014) were seemingly not transported from the SE China continental margin ~400 km away. This clearly implies that the accretionary prism may have been temporarily exposed and supplied clasts to the trench. The presence of red/purple-red, oxidized cements in the conglomerate also suggests that the source was partly subaerial. Therefore, the igneous pebbles were recycled during subaerial transport and/or temporary storage in a shoreline or shallow water environment before redeposition. Based on the accompanying pillow basalt and hyaloclastite breccia, which indicate a final submarine depositional setting for the Shihmen Conglomerate, the temporary emergence and exhumation of the accretionary prism can be attributed to seamount subduction (Figure 11a).

The detailed fieldwork and geochemical investigations in this study reveal that the mafic rocks dispersed in the argillaceous matrix of the Kenting Mélange exhibit similar lithological assemblages, geochemical diversity, and tectonic affinities as those in the Shihmen Conglomerate but are much more poorly sorted and differently rounded, indicating that they were accumulated under a tectonic regime distinct from the Shihmen Conglomerate. Despite the wide age distribution of microfossils in the Kenting Mélange, the most frequently obtained ages range from middle to late Miocene (C. P. Chang et al., 2009), indicating that the bulk mélange is composed of autochthonous blocks derived from the turbidite sequences east of the

Kenting Fault (Figure 3a). Similarly, based on the similar clay mineral polytypes between the Kenting Mélange and the Mutan Formation, S. B. Lin and Wang (2001) suggested that the former is basically a dismantled facies of the latter. Microfossils with Eocene to early Miocene ages (Chi, 1982) demonstrate that some components of the synrift deposits from grabens on the passive Asian continent were incorporated into the mélange. Younger microfossils with Pliocene to early Pleistocene ages suggest that the Kenting Mélange was produced due to the commencement of continental subduction and arc-continent collision (~4 Ma; Figure 11b) in southern Taiwan (C. Y. Huang et al., 2006), mainly through the intensive tectonic shearing of the accretionary complex (X. C. Zhang et al., 2016) and perhaps subordinate, landslides, which resulted in the slump deposits in the Cingwashih area.

7. Conclusions

In this study, we conducted systematic research on the accreted mafic rocks within the Hengchun accretionary prism to provide new constraints on their origins and to extract indicative information about the mantle nature and geodynamic evolution in the northern Manila subduction zone. Based on petrological, geochemical, isotopic, and geochronological analyses and comparisons with possible provenances, we arrive at the following conclusions.

1. The accreted mafic rocks exhibit significant geochemical variations and are identified as N-MORBs and alkaline OIBs originating from the subducting SCS and E-MORBs originating from the overriding Huatung Basin.
2. N-MORB-type rocks, which yield secondary ion mass spectrometry zircon U-Pb ages of 22.8 ± 0.3 and 24.2 ± 1.1 Ma, are derived from a virtually unmetasomatized DMM-like source.
3. Alkaline OIBs with HIMU-type Hf-Nd isotopic signatures are fragments of subducted seamounts. Their mantle source may have been derived from recycled oceanic crust components upwelled by the EMII-related Hainan Plume and metasomatized by DMM-like mantle. The lentiform Shihmen Conglomerate may have resulted from the temporary uplift and collapse of the accretionary prism caused by seamount subduction during the late Miocene.
4. The E-MORBs exhibit geochemical and Hf-Nd isotopic signatures similar to those of rocks from the Huatung Basin and yield an $^{40}Ar/^{39}Ar$ age of 135.0 ± 5.6 Ma. Accordingly, they were removed from the overriding plate due to the excessive shear stress between the converging plates and laterally transported by strike-slip movement; alternatively, they may have been scraped off from the subducted Luzon forearc slices.

Acknowledgments
This work was financially supported by the National Natural Science Foundation of China (grants 41606067, 41676048, U1701641, 41476036, and 41472093). The data supporting these conclusions can be found in supporting information Tables S1–S4 and Data Set S1.

References

Beccaluva, L., Ohnenstetter, D., & Ohnenstetter, M. (1979). Geochemical discrimination between ocean-floor and island-arc tholeiites: Application to some ophiolites. *Oxford Bulletin of Economics and Statistics*, *52*(2), 1874–1882. https://doi.org/10.1139/e79-172

Beck, M. E. (1983). On the mechanism of tectonic transport in zones of oblique subduction. *Tectonophysics*, *93*(1-2), 1–11. https://doi.org/10.1016/0040-1951(83)90230-5

Beck, M. E. (1986). Model for Late Mesozoic-Early Tertiary tectonics of coastal California and western Mexico and speculations on the origin of the San Andreas Fault. *Tectonics*, *5*, 49–64. https://doi.org/10.1029/TC005i001p00049

Bi, J. H., Ge, W. C., Yang, H., Wang, Z. H., Tian, D. X., Liu, X. W., et al. (2017). Geochemistry of MORB and OIB in the Yuejinshan Complex, NE China: Implications for petrogenesis and tectonic setting. *Journal of Asian Earth Sciences*, *145*(Part B), 475–493. https://doi.org/10.1016/j.jseaes.2017.06.025

Briais, A., Patriat, P., & Tapponnier, P. (1993). Updated interpretation of magnetic anomalies and seafloor spreading stages in the South China Sea: Implications for the Tertiary tectonics of Southeast Asia. *Journal of Geophysical Research*, *98*, 6299–6328. https://doi.org/10.1029/92JB02280

Byrne, T. (1998). Pre-collision kinematics and a possible modern analog for the Lichi and Kenting melanges, Taiwan. *Journal of the Geological Society of China*, *41*(4), 535–550.

Cabanis, B., & Lecolle, M. (1989). The La/10-Y/15-Nb/8 diagram: A tool for distinguishing volcanic series and discovering crustal mixing and/or contamination. *Comptes Rendus de l'Academie des Sciences*, *309*(20), 2023–2029.

Chang, C. P., Angelier, J., & Huang, C. Y. (2009). Evolution of subductions indicated by Mélanges in Taiwan. In S. Lallemand & F. Funiciello (Eds.), *Subduction zone geodynamics* (Vol. 5, pp. 207–225). Berlin, Heidelberg: Springer. https://doi.org/10.1007/978-3-540-87974-9_11

Chang, C. P., Angelier, J., Lee, T. Q., & Huang, C. Y. (2003). From continental margin extension to collision orogen: Structural development and tectonic rotation of the Hengchun peninsula, southern Taiwan. *Tectonophysics*, *361*(1–2), 61–82. https://doi.org/10.1016/S0040-1951(02)00561-9

Chang, L. S. (1964). A biostratigraphic study of the Tertiary in the Hengchun peninsula, Taiwan, based on smaller Foraminifera (I. Northern Part). *Proceedings of Geological Society of China*, *7*, 48–62.

Chauvel, C., Lewin, E., Carpentier, M., Arndt, N. T., & Marini, J. C. (2007). Role of recycled oceanic basalt and sediment in generating the Hf–Nd mantle array. *Nature Geoscience*, *1*(1), 64–67. https://doi.org/10.1038/ngeo.2007.51

Chen, H. Y., Yang, H. J., Liu, Y. H., Huang, K. F., & Takazawa, E. (2018). Tectonic affinities of the accreted basalts in southern Taiwan. *Journal of Asian Earth Sciences*, *158*, 253–265. https://doi.org/10.1016/j.jseaes.2018.02.015

Chen, L., Hu, J., Yang, D., Song, H., & Wang, Z. (2017). Kinematic models for the opening of the South China Sea: An upwelling divergent flow origin. *Journal of Geodynamics*, *107*, 20–33. https://doi.org/10.1016/j.jog.2017.03.002

Cheng, W. B. (2009). Tomographic imaging of the convergent zone in eastern Taiwan—A subducting forearc sliver revealed? *Tectonophysics*, *466*(3-4), 170–183. https://doi.org/10.1016/j.tecto.2007.11.010

Chi, W. R. (1982). The calcareous nannofossils of the Lichi mélange and the Kenting mélange and their significance in the interpretation of plate tectonics of the Taiwan region. *Ti-Chih (Geology)*, *4*(1), 99–112.

Collerson, K. D., Williams, Q., Ewart, A. E., & Murphy, D. T. (2010). Origin of HIMU and EM-1 domains sampled by ocean island basalts, kimberlites and carbonatites: The role of CO_2-fluxed lower mantle melting in thermochemical upwellings. *Physics of the Earth and Planetary Interiors*, *181*(3-4), 112–131. https://doi.org/10.1016/j.pepi.2010.05.008

Corfu, F. (2013). A century of U-Pb geochronology: The long quest towards concordance. *Bulletin of the Geological Society of America*, *125*(1–2), 33–47. https://doi.org/10.1130/B30698.1

Dasgupta, R., Hirschmann, M. M., & Smith, N. D. (2007). Partial melting experiments of peridotite + CO_2 at 3 GPa and genesis of alkalic ocean island basalts. *Journal of Petrology*, *48*(11), 2093–2124. https://doi.org/10.1093/petrology/egm053

Deschamps, A., & Lallemand, S. (2002). The West Philippine Basin: An Eocene to early Oligocene back arc basin opened between two opposed subduction zones. *Journal of Geophysical Research*, *107*(B12), 2322. https://doi.org/10.1029/2001JB001706

Deschamps, A., Monié, P., Lallemand, S., Hsu, S. K., & Yeh, K. Y. (2000). Evidence for Early Cretaceous oceanic crust trapped in the Philippine Sea Plate. *Earth and Planetary Science Letters*, *179*(3–4), 503–516. https://doi.org/10.1016/S0012-821X(00)00136-9

Dominguez, S., Malavieille, J., & Lallemand, S. E. (2000). Deformation of accretionary wedges in response to seamount subduction: Insights from sandbox experiments. *Tectonics*, *19*, 182–196. https://doi.org/10.1029/1999TC900055

Eakin, D. H., McIntosh, K. D., Van Avendonk, H. J. A., & Lavier, L. (2015). New geophysical constraints on a failed subduction initiation: The structure and potential evolution of the Gagua Ridge and Huatung Basin. *Geochemistry, Geophysics, Geosystems*, *16*, 380–400. https://doi.org/10.1002/2014GC005548

Foland, K. A., Linder, J. S., Laskowski, T. E., & Grant, N. K. (1984). $^{40}Ar^{39}Ar$ dating of glauconites: Measured ^{39}Ar recoil loss from well-crystallized specimens. *Chemical Geology*, *46*(3), 241–264. https://doi.org/10.1016/0009-2541(84)90192-X

Giletycz, S., Loget, N., Chang, C. P., & Mouthereau, F. (2015). Transient fluvial landscape and preservation of low-relief terrains in an emerging orogen: Example from Hengchun Peninsula, Taiwan. *Geomorphology*, *231*, 169–181. https://doi.org/10.1016/j.geomorph.2014.11.026

Giletycz, S. J., Chang, C.-P., Lin, A. T.-S., Ching, K.-E., & Shyu, J. B. H. (2017). Improved alignment of the Hengchun Fault (southern Taiwan) based on fieldwork, structure-from-motion, shallow drilling, and levelling data. *Tectonophysics*, *721*, 435–447. https://doi.org/10.1016/j.tecto.2017.10.018

Hartmann, L. A., & Santos, J. O. S. (2004). Predominance of high Th/U, magmatic zircon in Brazilian Shield sandstones. *Geology*, *32*(1), 73–76. https://doi.org/10.1130/G20007.1

Hernandez Almeida, I. (2014). South China Sea tectonics. Opening of the South China Sea and its implications for Southeast Asian tectonics, climates, and deep mantle processes since the late Mesozoic (International Ocean Discovery Program Preliminary Report 349). https://doi.org/10.14379/iodp.pr.349.2014

Hickey-Vargas, R., Bizimis, M., & Deschamps, A. (2008). Onset of the Indian Ocean isotopic signature in the Philippine Sea Plate: Hf and Pb isotope evidence from Early Cretaceous terranes. *Earth and Planetary Science Letters*, *268*(3–4), 255–267. https://doi.org/10.1016/j.epsl.2008.01.003

Hofmann, A. W. (1988). Chemical differentiation of the Earth: The relationship between mantle, continental crust, and oceanic crust. *Earth and Planetary Science Letters*, *90*(3), 297–314. https://doi.org/10.1016/0012-821X(88)90132-X

Hosseini, M. R., Hassanzadeh, J., Alirezaei, S., Sun, W. D., & Li, C. Y. (2017). Age revision of the Neotethyan arc migration into the southeast Urumieh-Dokhtar belt of Iran: Geochemistry and U–Pb zircon geochronology. *Lithos*, *284*, 296–309. https://doi.org/10.1016/j.lithos.2017.03.012

Hsu, S. K., Yeh, Y. C., Doo, W. B., & Tsai, C. H. (2004). New bathymetry and magnetic lineations identifications in the northernmost South China Sea and their tectonic implications. *Marine Geophysical Researches*, *25*(1–2), 29–44. https://doi.org/10.1007/s11001-005-0731-7

Huang, C. Y. (1984). Some planktic foraminifers from the olistostromes of the Kenting Formation, southern Hengchun Peninsula. *Acta Geologica*, *22*, 22–34.

Huang, C. Y., Cheng, Y. M., & Jeh, C. C. (1985). Genesis of the Kenting Formation in the Hengchun Peninsula, southern Taiwan. *Ti-Chih (Geology)*, *6*(1), 21–38.

Huang, C. Y., Wu, W. Y., Chang, C. P., Tsao, S., Yuan, P. B., Lin, C. W., & Xia, K. Y. (1997). Tectonic evolution of accretionary prism in the arc-continent collision terrane of Taiwan. *Tectonophysics*, *281*(1–2), 31–51. https://doi.org/10.1016/S0040-1951(97)00157-1

Huang, C. Y., Xia, K. Y., Yuan, P. B., & Chen, P. G. (2001). Structural evolution from Paleogene extension to Latest Miocene-Recent arc-continent collision offshore Taiwan: Comparison with on land geology. *Journal of Asian Earth Sciences*, *19*(5), 619–638. https://doi.org/10.1016/S1367-9120(00)00065-1

Huang, C. Y., Yen, Y., Zhao, Q. H., & Lin, C. T. (2012). Cenozoic stratigraphy of Taiwan: Window into rifting, stratigraphy and paleoceanography of South China Sea. *Chinese Science Bulletin*, *57*(24), 3130–3149. https://doi.org/10.1007/s11434-012-5349-y

Huang, C. Y., Yuan, P. B., Lin, C. W., Wang, T. K., & Chang, C. P. (2000). Geodynamic processes of Taiwan arc-continent collision and comparison with analogs in Timor, Papua New Guinea, Urals and Corsica. *Tectonophysics*, *325*(1–2), 1–21. https://doi.org/10.1016/S0040-1951(00)00128-1

Huang, C. Y., Yuan, P. B., & Tsao, S. J. (2006). Temporal and spatial records of active arc-continent collision in Taiwan: A synthesis. *Geological Society of America Bulletin*, *118*(3–4), 274–288. https://doi.org/10.1130/B25527.1

Huang, X. L., Niu, Y. L., Xu, Y. G., Ma, J. L., Qiu, H. N., & Zhong, J. W. (2013). Geochronology and geochemistry of Cenozoic basalts from eastern Guangdong, SE China: Constraints on the lithosphere evolution beneath the northern margin of the South China Sea. *Contributions to Mineralogy and Petrology*, *165*(3), 437–455. https://doi.org/10.1007/s00410-012-0816-7

Humphris, S. E. (1984). The mobility of the rare earth elements in the crust. *Developments in Geochemistry*, *2*(9), 317–342. https://doi.org/10.1016/B978-0-444-42148-7.50014-9

Isozaki, Y., Maruyama, S., & Furuoka, F. (1990). Accreted oceanic materials in Japan. *Tectonophysics*, *181*(1-4), 179–205. https://doi.org/10.1016/0040-1951(90)90016-2

Jiang, Z., Wang, D., Zhang, Z., Duan, S., Kang, Y., & Li, F. (2018). Application of in situ titanite U–Pb geochronology to volcanic-hosted magnetite deposit: New constraints on the timing and genesis of the Zhibo deposit, Western Tianshan, NW China. *Ore Geology Reviews*, *95*, 325–341. https://doi.org/10.1016/j.oregeorev.2018.03.001

Kempton, P. D., Pearce, J. A., Barry, T. L., Fitton, J. G., Langmuir, C., & Christie, D. M. (2002). Sr-Nd-Pb-Hf isotope results from ODP leg 187: Evidence for mantle dynamics of the Australian-Antarctic discordance and origin of the Indian MORB source. *Geochemistry, Geophysics, Geosystems*, *3*(12), 1074. https://doi.org/10.1029/2002GC000320

Ker, C. M., Yang, H. J., Zhang, J. X., Shau, Y. H., Chieh, C. J., Meng, F. C., et al. (2015). Compositional and Sr–Nd–Hf isotopic variations of Baijingsi eclogites from the North Qilian orogen, China: Causes, protolith origins, and tectonic implications. *Gondwana Research*, *28*(2), 721–734. https://doi.org/10.1016/j.gr.2014.06.006

Khogenkumar, S., Singh, A. K., Bikramaditya Singh, R. K., Khanna, P. P., Singh, N. I., & Singh, W. I. (2016). Coexistence of MORB and OIB-type mafic volcanics in the Manipur Ophiolite Complex, Indo-Myanmar Orogenic Belt, northeast India: Implication for heterogeneous mantle source at the spreading zone. *Journal of Asian Earth Sciences*, *116*(C), 42–58. https://doi.org/10.1016/j.jseaes.2015.11.007

Kirstein, L. A., Carter, A., & Chen, Y.-G. (2010). Testing inferences from palaeocurrents: Application of zircon double-dating to Miocene sediments from the Hengchun Peninsula, Taiwan. *Terra Nova*, *22*(6), 483–493. https://doi.org/10.1111/j.1365-3121.2010.00970.x

Koppers, A. A. P. (2002). ArArCALC—Software for $^{40}Ar/^{39}Ar$ age calculations. *Computers & Geosciences*, *28*(5), 605–619. https://doi.org/10.1016/S0098-3004(01)00095-4

Lai, Y. M., Song, S. R., Lo, C. H., Lin, T. H., Chu, M. F., & Chung, S. L. (2017). Age, geochemical and isotopic variations in volcanic rocks from the Coastal Range of Taiwan: Implications for magma generation in the Northern Luzon Arc. *Lithos*, *272-273*, 92–115. https://doi.org/10.1016/j.lithos.2016.11.012

Lan, Q., Yan, Y., Huang, C. Y., Santosh, M., Shan, Y. H., Chen, W., et al. (2015). Topographic architecture and drainage reorganization in Southeast China: Zircon U-Pb chronology and Hf isotope evidence from Taiwan. *Gondwana Research*, *36*(24), 376–389. https://doi.org/10.1016/j.gr.2015.07.008

Le Maitre, R. W. (2002). Igneous rocks: A classification and glossary of terms, 1(70), 93–120, DOI: https://doi.org/10.1017/CBO9780511535581

Lewis, J. C., O'Hara, D. J., & Rau, R.-J. (2015). Seismogenic strain across the transition from fore-arc slivering to collision in southern Taiwan. *Journal of Geophysical Research: Solid Earth*, *120*, 4539–4555. https://doi.org/10.1002/2015JB011906

Li, C. F., Xu, X., Lin, J., Sun, Z., Zhu, J., Yao, Y. J., et al. (2014). Ages and magnetic structures of the South China Sea constrained by deep tow magnetic surveys and IODP Expedition 349. *Geochemistry, Geophysics, Geosystems*, *15*, 4958–4983. https://doi.org/10.1002/2014GC005567

Li, P., & Rao, C. (1994). Tectonic characteristics and evolution history of the Pearl river mouth basin. *Tectonophysics*, *235*(1–2), 13–25. https://doi.org/10.1016/0040-1951(94)90014-0

Li, X. H. (2003). Neoproterozoic granitoids in South China: Crustal melting above a mantle plume at ca. 825 Ma? *Precambrian Research*, *122*(1), 45–83. https://doi.org/10.1016/S0301-9268(02)00207-3

Li, X. H., Liu, Y., Li, Q. L., Guo, C. H., & Chamberlain, K. R. (2009). Precise determination of Phanerozoic zircon Pb/Pb age by multicollector SIMS without external standardization. *Geochemistry, Geophysics, Geosystems*, *10*, Q04010. https://doi.org/10.1029/2009GC002400

Li, X. H., Liu, Y., Yang, Y. H., Chen, F. K., Tu, X. L., & Qi, C. S. (2007). Rapid separation of Lu-Hf and Sm-Nd from a single rock dissolution and precise measurement of Hf-Nd isotopic ratios for national rock standards. *Acta Petrologica Sinica*, *23*(2), 221–226. https://doi.org/10.3969/j.issn.1000-0569.2007.02.002

Li, X. H., Qi, C. S., Liu, Y., Liang, X. R., Tu, X. L., Xie, L. W., & Yang, Y. H. (2005). Rapid separation of Hf from rock samples for isotope analysis by MC-ICPMS: A modified single-column extraction chromatography method. *Geochimica*, *34*(2), 109–114. https://doi.org/10.3321/j.issn:0379-1726.2005.02.002

Liang, Q., Jing, H., & Gregoire, D. C. (2000). Determination of trace elements in granites by inductively coupled plasma mass spectrometry. *Talanta*, *51*(3), 507–513. https://doi.org/10.1016/S0039-9140(99)00318-5

Lin, A. T., Yao, B. C., Hsu, S. K., Liu, C. S., & Huang, C. Y. (2009). Tectonic features of the incipient arc-continent collision zone of Taiwan: Implications for seismicity. *Tectonophysics*, *479*(1–2), 28–42. https://doi.org/10.1016/j.tecto.2008.11.004

Lin, S. B., & Wang, Y. R. (2001). Clay minerals in the rock formations on the Hengchun Peninsula, southern Taiwan, and their tectonic implications. *Western Pacific Earth Sciences*, *1*(2), 157–174.

Liu, C. S., Liu, S. Y., Kuo, B. Y., Lundberg, N., & Reed, D. L. (1992). Characteristics of the gravity and magnetic anomalies off southern Taiwan. *Acta Geologica Taiwanica*, *30*, 123–130.

Ludwig, K. R. (2008). User's manual for Isoplot/Ex: A geochronological toolkit for Microsoft Excel. *Department of Computer Science University of Canterbury*, *130*(3), 206–207.

Ma, J., Wei, G., Liu, Y., Ren, Z., Xu, Y., & Yang, Y. (2013). Precise measurement of stable neodymium isotopes of geological materials by using MC-ICP-MS. *Journal of Analytical Atomic Spectrometry*, *28*(12), 1926–1931. https://doi.org/10.1039/c3ja50229e

MacDougall, J. D., Finkel, R. C., Carlson, J., & Krishnaswami, S. (1979). Isotopic evidence for uranium exchange during low-temperature alteration of oceanic basalt. *Earth and Planetary Science Letters*, *42*(1), 27–34. https://doi.org/10.1016/0012-821X(79)90187-0

Malavieille, J., Lallemand, S., Dominguez, S., Deschamps, A., Lu, C. Y., Liu, C. S., et al., & the, A. C. T. Scientific Crew (2002). Arc-continent collision in Taiwan: New marine observations and tectonic evolution. *Geological Society of America Special Papers*, *358*, 189–213. https://doi.org/10.1130/0-8137-2358-2.187

Malavieille, J., Molli, G., Genti, M., Dominguez, S., Beyssac, O., Taboada, A., et al. (2016). Formation of ophiolite-bearing tectono-sedimentary mélanges in accretionary wedges by gravity driven submarine erosion: Insights from analogue models and case studies. *Journal of Geodynamics*, *100*, 87–103. https://doi.org/10.1016/j.jog.2016.05.008

Malavieille, J., & Trullenque, G. (2009). Consequences of continental subduction on forearc basin and accretionary wedge deformation in SE Taiwan: Insights from analogue modeling. *Tectonophysics*, *466*(3-4, 377–394. https://doi.org/10.1016/j.tecto.2007.11.016)

Meschede, M. (2014). Accretionary wedge. In J. Harff, M. Meschede, S. Petersen, & J. Thiede (Eds.), *Encyclopedia of marine geosciences* (Vol. A, pp. 1–5). Dordrecht, Netherlands: Springer. https://doi.org/10.1007/978-94-007-6644-0_101-1

Muller, C., Pelletier, B., Schaaf, A., Glacon, G., & Huang, T. C. (1984). Age determination of the ophiolitic materials from the Hengchun Peninsula (South Taiwan) and their tectonic implication. *Memoir of Geological Society of China*, *6*, 327–333.

Nebel, O., Arculus, R. J., van Westrenen, W., Woodhead, J. D., Jenner, F. E., Nebel-Jacobsen, Y. J., et al. (2013). Coupled Hf–Nd–Pb isotope co-variations of HIMU oceanic island basalts from Mangaia, Cook-Austral islands, suggest an Archean source component in the mantle transition zone. *Geochimica et Cosmochimica Acta*, *112*(3), 87–101. https://doi.org/10.1016/j.gca.2013.03.005

Niu, Y., & O'Hara, M. J. (2003). Origin of ocean island basalts: A new perspective from petrology, geochemistry, and mineral physics considerations. *Journal of Geophysical Research*, *108*(B4), 2209. https://doi.org/10.1029/2002JB002048

Okamura, Y. (1991). Large-scale mélange formation due to seamount subduction: An example from the Mesozoic accretionary complex in central Japan. *Journal of Geology*, *99*(5), 661–674. https://doi.org/10.1086/629531

Orihashi, Y., Maeda, J., Tanaka, R., Zeniya, R., & Niida, K. (1998). Sr and Nd isotopic data for the seven GSJ rock reference samples: JA-1, JB-1a, JB-2, JB-3, JG-1a, JGb-1, and JR-1. *Geochemical Journal*, *32*(3), 205–211. https://doi.org/10.2343/geochemj.32.205

Page, B. M., & Lan, C. Y. (1983). The Kenting Mélange and its record of tectonic events. *Memoir of Geological Society of China*, *5*, 227–248.

Pearce, J. A. (1983). Role of the sub-continental lithosphere in magma genesis at active continental margins. *Continental Basalts and Mantle Xenoliths*, *147*(6), 230–249.

Pearce, J. A. (2008). Geochemical fingerprinting of oceanic basalts with applications to ophiolite classification and the search for Archean oceanic crust. *Lithos*, *100*(1–4), 14–48. https://doi.org/10.1016/j.lithos.2007.06.016

Pearce, J. A., Kempton, P. D., & Gill, J. B. (2007). Hf–Nd evidence for the origin and distribution of mantle domains in the SW Pacific. *Earth and Planetary Science Letters*, *260*(1–2), 98–114. https://doi.org/10.1016/j.epsl.2007.05.023

Pearce, J. A., & Norry, M. J. (1979). Petrogenetic implications of Ti, Zr, Y, and Nb variations in volcanic rocks. *Contributions to Mineralogy and Petrology*, *69*(1), 33–47. https://doi.org/10.1007/BF00375192

Pearce, J. A., & Stern, R. J. (2006). Origin of back-arc basin magmas: Trace element and isotope perspectives. In D. M. Christie, C. R. Fisher, S. M. Lee, & S. Givens (Eds.), *Back-arc spreading systems: Geological, biological, chemical, and physical interactions* (Vol. 166, pp. 63–68). Washington, DC: American Geophysical Union. https://doi.org/10.1029/166GM06

Pelletier, B., & Stephan, J. F. (1986). Middle miocene deduction and late miocene beginning of collision registered in the hengchun peninsula: Geodynamic implications for the evolution of Taiwan. *Tectonophysics*, *125*(1–3), 133–160. https://doi.org/10.1016/0040-1951(86)90011-9

Qi, L., & Zhou, M. F. (2008). Determination of platinum-group elements in OPY-1: Comparison of results using different digestion techniques. *Geostandards and Geoanalytical Research*, *32*(3), 377–387. https://doi.org/10.1111/j.1751-908X.2008.00893.x

Qiu, H. N., & Jiang, Y. D. (2007). Sphalerite $^{40}Ar/^{39}Ar$ progressive crushing and stepwise heating techniques. *Earth and Planetary Science Letters*, *256*(1-2), 224–232. https://doi.org/10.1016/j.epsl.2007.01.028

Renne, P. R., Swisher, C. C., Deino, A. L., Karner, D. B., Owens, T. L., & DePaolo, D. J. (1998). Intercalibration of standards, absolute ages and uncertainties in $^{40}Ar/^{39}Ar$ dating. *Chemical Geology*, *145*(1-2), 117–152. https://doi.org/10.1016/S0009-2541(97)00159-9

Rollinson, H. R. (1993). *Using geochemical data: Evaluation, presentation, interpretation*. New York: Longman Scientific Technical.

Rubatto, D. (2002). Zircon trace element geochemistry: Partitioning with garnet and the link between U–Pb ages and metamorphism. *Chemical Geology*, *184*(1-2), 123–138. https://doi.org/10.1016/S0009-2541(01)00355-2

Rudnick, R. L., & Gao, S. (2003). Composition of the continental crust. In K. K. Turekian (Ed.), *Treatise on geochemistry* (pp. 1–64). Pergamon: Oxford. https://doi.org/10.1016/B0-08-043751-6/03016-4

Saccani, E., Allahyari, K., & Rahimzadeh, B. (2014). Petrology and geochemistry of mafic magmatic rocks from the Sarve-Abad ophiolites (Kurdistan region, Iran): Evidence for interaction between MORB-type asthenosphere and OIB-type components in the southern Neo-Tethys Ocean. *Tectonophysics*, *621*(Supplement C), 132–147. https://doi.org/10.1016/j.tecto.2014.02.011

Safonova, I., Maruyama, S., Kojima, S., Komiya, T., Krivonogov, S., & Koshida, K. (2016). Recognizing OIB and MORB in accretionary complexes: A new approach based on ocean plate stratigraphy, petrology and geochemistry. *Gondwana Research*, *33*(Supplement C), 92–114. https://doi.org/10.1016/j.gr.2015.06.013

Said, N., & Kerrich, R. (2009). Geochemistry of coexisting depleted and enriched Paringa Basalts, in the 2.7 Ga Kalgoorlie Terrane, Yilgarn Craton, Western Australia: Evidence for a heterogeneous mantle plume event. *Precambrian Research*, *174*(3–4), 287–309. https://doi.org/10.1016/j.precamres.2009.08.002

Saito, T., Uno, M., Sato, T., Fujisaki, W., Haraguchi, S., Li, Y. B., et al. (2015). Geochemistry of accreted metavolcanic rocks from the Neoproterozoic Gwna Group of Anglesey–Lleyn, NW Wales, U.K.: MORB and OIB in the Iapetus Ocean. *Tectonophysics*, *662*(3), 243–255. https://doi.org/10.1016/j.tecto.2015.08.015

Salters, V. J. M., Mallick, S., Hart, S. R., Langmuir, C. E., & Stracke, A. (2011). Domains of depleted mantle: New evidence from hafnium and neodymium isotopes. *Geochemistry, Geophysics, Geosystems*, *12*, Q08001. https://doi.org/10.1029/2011GC003617

Salters, V. J. M., & White, W. M. (1998). Hf isotope constraints on mantle evolution. *Chemical Geology*, *145*(3–4), 447–460. https://doi.org/10.1016/S0009-2541(97)00154-X

Sano, H., & Kanmero, K. (1991). Collapse of ancient oceanic reef complex-what happened during collision of Akiyoshi reef complex?—Sequence of collisional collapse and generation of collapse products. *Journal of the Geological Society of Japan*, *97*(8), 631–644_3. https://doi.org/10.5575/geosoc.97.631

Saunders, A. D., Tarney, J., Kerr, A. C., & Kent, R. W. (1996). The formation and fate of large oceanic igneous provinces. *Lithos*, *37*(2-3), 81–95. https://doi.org/10.1016/0024-4937(95)00030-5

Shan, Y. H., Nie, G. J., Yan, Y., & Huang, C. Y. (2013). The transition from the passive to active continental margin: A case study of brittle fractures in the Miocene Loshui Sandstone on the Hengchun Peninsula, southern Taiwan. *Tectonics*, *32*, 65–79. https://doi.org/10.1029/2012TC003178

Shao, W. Y., Chung, S. L., Chen, W. S., Lee, H. Y., & Xie, L. W. (2015). Old continental zircons from a young oceanic arc, eastern Taiwan: Implications for Luzon subduction initiation and Asian accretionary orogeny. *Geology*, *43*(6), 479–482. https://doi.org/10.1130/G36499.1

Shervais, J. W. (1982). Ti-V plots and the petrogenesis of modern and ophiolitic lavas. *Earth and Planetary Science Letters*, *59*(1), 101–118. https://doi.org/10.1016/0012-821X(82)90120-0

Shyu, J. B. H., Wu, Y. M., Chang, C. H., & Huang, H. H. (2011). Tectonic erosion and the removal of forearc lithosphere during arc-continent collision: Evidence from recent earthquake sequences and tomography results in eastern Taiwan. *Journal of Asian Earth Sciences*, *42*(3), 415–422. https://doi.org/10.1016/j.jseaes.2011.05.015

Song, S. R., & Lo, H. J. (2002). Lithofacies of volcanic rocks in the central Coastal Range, eastern Taiwan: Implications for island arc evolution. *Journal of Asian Earth Sciences*, *21*(1), 23–38. https://doi.org/10.1016/S1367-9120(02)00003-2

Sun, S. S., & McDonough, W. F. (1989). Chemical and isotopic systematics of oceanic basalts: Implications for mantle composition and processes. *Geological Society, London, Special Publications*, *42*(1), 313–345. https://doi.org/10.1144/GSL.SP.1989.042.01.19

Sung, Q., & Wang, Y. (1986). Sedimentary environments of the Miocene sediments in the Hengchun Peninsula and their tectonic implication. *Memoir of Geological Society of China*, *7*, 325–340.

Tanaka, T., Togashi, S., Kamioka, H., Amakawa, H., Kagami, H., Hamamoto, T., et al. (2000). JNdi-1: A neodymium isotopic reference in consistency with LaJolla neodymium. *Chemical Geology*, *168*(3-4), 279–281. https://doi.org/10.1016/S0009-2541(00)00198-4

Tatsumi, Y., & Ishizaka, K. (1981). Existence of andesitic primary magma: An example from southwest Japan. *Earth and Planetary Science Letters*, *53*(1), 124–130. https://doi.org/10.1016/0012-821X(81)90033-9

Taylor, B., & Hayes, D. E. (1983). Origin and history of the South China Sea basin. In D. E. Hayes (Ed.), *Geophysical monograph* (Vol. 27, pp. 23–56). Washington DC: American Geophysical Union. https://doi.org/10.1029/GM027p0023

Tera, F., & Wasserburg, G. J. (1972). U-Th-Pb systematics in three Apollo 14 basalts and the problem of initial Pb in lunar rocks. *Earth and Planetary Science Letters*, *14*(3), 281–304. https://doi.org/10.1016/0012-821X(72)90128-8

Tsai, C. H. (2017). *Tectonic development and sediment provenances of the Luzon Island and Hengchun Peninsula from detrital zircon analysis* (Master dissertation). Taipei City: National Taiwan University.

Tsai, C. H., & Shyu, J. B. H. (2015). *Detrital zircon analysis of Miocene series of the Hengchun Peninsula, southern Taiwan*. Paper Presented at 2015 AGU Fall Meeting, San Francisco, CA.

Turner, G., & Cadogan, P. H. (1974). Possible effects of ^{39}Ar recoil in ^{40}Ar-^{39}Ar dating. *Geochimica et Cosmochimica Acta*, *2*(5), 1601–1615.

Ueda, H., Kawamura, M., & Yoshida, K. (2002). Blueschist-bearing fluvial conglomerate and unconformity in the Cretaceous forearc sequence, south central Hokkaido, northern Japan: Rapid exhumation of a high-P/T metamorphic accretionary complex. *Journal of the Geological Society of Japan*, *108*(3), 133–152. https://doi.org/10.5575/geosoc.108.133

Vannucchi, P., Sage, F., Phipps Morgan, J., Remitti, F., & Collot, J.-Y. (2012). Toward a dynamic concept of the subduction channel at erosive convergent margins with implications for interplate material transfer. *Geochemistry, Geophysics, Geosystems*, *13*, Q02003. https://doi.org/10.1029/2011GC003846

Vervoort, J. D., Patchett, P. J., Blichert Toft, J., & Albarède, F. (1999). Relationships between Lu–Hf and Sm–Nd isotopic systems in the global sedimentary system. *Earth and Planetary Science Letters*, *168*(1–2), 79–99. https://doi.org/10.1016/S0012-821X(99)00047-3

Von Huene, R., Ranero, C. R., & Vannucchi, P. (2004). Generic model for subduction erosion. *Geology*, *32*(10), 913–916. https://doi.org/10.1130/G20563.1

Von Huene, R., Ranero, C. R., Weinrebe, W., & Hinz, K. (2000). Quaternary convergent margin tectonics of Costa Rica, segmentation of the Cocos Plate, and Central American volcanism. *Tectonics*, *19*, 314–334. https://doi.org/10.1029/1999TC001143

Wang, X., Wu, M., Liang, D., & Yin, A. (1985). Some geochemical characteristics of basalts in the South China Sea. *Chinese Journal of Geochemistry*, *4*(4), 380–390. https://doi.org/10.1007/bf02843275

Wang, X. J., Liu, J. Q., & Chen, L. H. (2014). Geochemical characteristics of HIMU-type oceanic island basalts. *Geological Journal of China Universities*, *20*(3), 353–367. https://doi.org/10.16108/j.issn1006-7493.2014.03.019

Wiedenbeck, M., AllÉ, P., Corfu, F., Griffin, W. L., Meier, M., Oberli, F., et al. (1995). Three natural zircon standards for U-Th-Pb, Lu-Hf, trace element and REE analyses. *Geostandards Newsletter*, *19*(1), 1–23. https://doi.org/10.1111/j.1751-908X.1995.tb00147.x

Williams, I. S. (1998). U-Th-Pb geochronology by ion microprobe. *Applications of Microanalytical Techniques to Understanding Mineralizing Processes*, *7*, 1–35. https://doi.org/10.1080/00241160410006483

Winchester, J., & Floyd, P. (1977). Geochemical discrimination of different magma series and their differentiation products using immobile elements. *Chemical Geology*, *20*(4), 325–343. https://doi.org/10.1016/0009-2541(77)90057-2

Wood, D. A. (1980). The application of a Th-Hf-Ta diagram to problems of tectonomagmatic classification and to establishing the nature of crustal contamination of basaltic lavas of the British Tertiary volcanic province. *Earth and Planetary Science Letters*, *50*, 11–30. https://doi.org/10.1016/0012-821X(80)90116-8

Wu, F. Y., Yang, Y. H., Xie, L. W., Yang, J. H., & Xu, P. (2006). Hf isotopic compositions of the standard zircons and baddeleyites used in U–Pb geochronology. *Chemical Geology*, *234*(1-2), 105–126. https://doi.org/10.1016/j.chemgeo.2006.05.003

Yan, Q., Castillo, P., Shi, X., Wang, L., Liao, L., & Ren, J. (2015). Geochemistry and petrogenesis of volcanic rocks from Daimao Seamount (South China Sea) and their tectonic implications. *Lithos*, *218-219*, 117–126. https://doi.org/10.1016/j.lithos.2014.12.023

Yan, Q., Shi, X., & Castillo, P. R. (2014). The late Mesozoic–Cenozoic tectonic evolution of the South China Sea: A petrologic perspective. *Journal of Asian Earth Sciences*, *85*(2), 178–201. https://doi.org/10.1016/j.jseaes.2014.02.005

Yan, Q., Shi, X., Metcalfe, I., Liu, S., Xu, T., Kornkanitnan, N., et al. (2018). Hainan mantle plume produced late Cenozoic basaltic rocks in Thailand, Southeast Asia. *Scientific Reports*, *8*(1), 2640. https://doi.org/10.1038/s41598-018-20712-7

Yan, Q., Shi, X., Wang, K., Bu, W., & Xiao, L. (2008). Major element, trace element, and Sr, Nd and Pb isotope studies of Cenozoic basalts from the South China Sea. *Science in China Series D: Earth Sciences*, *51*(4), 550–566. https://doi.org/10.1007/s11430-008-0026-3

Yang, G., Li, Y., Santosh, M., Gu, P., Yang, B., Zhang, B., et al. (2012). A Neoproterozoic seamount in the Paleoasian Ocean: Evidence from zircon U–Pb geochronology and geochemistry of the Mayile ophiolitic mélange in West Junggar, NW China. *Lithos*, *140-141*, 53–65. https://doi.org/10.1016/j.lithos.2012.01.026

Yang, G., Li, Y., Xiao, W., & Tong, L. (2015). OIB-type rocks within West Junggar ophiolitic mélanges: Evidence for the accretion of sea-mounts. *Earth-Science Reviews*, *150*(c), 477–496. https://doi.org/10.1016/j.earscirev.2015.09.002

Yang, L., Wang, F., Feng, H., Wu, L., & Shi, W. (2014). ^{40}Ar/^{39}Ar geochronology of Holocene volcanic activity at Changbaishan Tianchi volcano, Northeast China. *Quaternary Geochronology*, *21*(1), 106–114. https://doi.org/10.1016/j.quageo.2013.10.008

Yu, M. M., Yan, Y., Huang, C. Y., Zhang, X. C., Tian, Z. X., Chen, W. H., & Santosh, M. (2018). Opening of the South China Sea and upwelling of the Hainan Plume. *Geophysical Research Letters*, *45*, 2600–2609. https://doi.org/10.1002/2017GL076872

Yuan, C., Sun, M., Wilde, S., Xiao, W., Xu, Y., Long, X., & Zhao, G. (2010). Post-collisional plutons in the Balikun area, East Chinese Tianshan: Evolving magmatism in response to extension and slab break-off. *Lithos*, *119*(3-4), 269–288. https://doi.org/10.1016/j.lithos.2010.07.004

Zhang, G. L., Chen, L. H., Jackson, M. G., & Hofmann, A. W. (2017). Evolution of carbonated melt to alkali basalt in the South China Sea. *Nature Geoscience*, *10*(3), 229–235. https://doi.org/10.1038/ngeo2877

Zhang, G. L., Luo, Q., Zhao, J., Jackson, M. G., Guo, L. S., & Zhong, L. F. (2018). Geochemical nature of sub-ridge mantle and opening dynamics of the South China Sea. *Earth and Planetary Science Letters*, *489*, 145–155. https://doi.org/10.1016/j.epsl.2018.02.040

Zhang, X. C., Cawood, P. A., Huang, C. Y., Wang, Y. J., Yan, Y., Santosh, M., et al. (2016). From convergent plate margin to arc-continent collision: Formation of the Kenting Mélange, southern Taiwan. *Gondwana Research*, *38*, 171–182. https://doi.org/10.1016/j.gr.2015.11.010

Zhang, X. C., Yan, Y., Huang, C. Y., Chen, D. F., Shan, Y. H., Lan, Q., et al. (2014). Provenance analysis of the Miocene accretionary prism of the Hengchun Peninsula, southern Taiwan, and regional geological significance. *Journal of Asian Earth Sciences*, *85*(2), 26–39. https://doi.org/10.1016/j.jseaes.2014.01.021